NONLINEAR FINITE ELEMENT MODEL ANALYSIS OF HUMAN

ACCOMMODATION LENS

by

TRI LE

Presented to the Faculty of the Graduate School of

The University of Texas at Arlington in Partial Fulfillment

of the Requirements

for the Degree of

MASTER OF SCIENCE IN CIVIL ENGINEERING

THE UNIVERSITY OF TEXAS AT ARLINGTON

August 2005

ACKNOWLEDGEMENTS

I wish to express my sincere thanks to Dr. Ali Abolmaali for his guidance and remarkable patience throughout the supervision of this research. I am also grateful thanks to Dr. Ali Abolmaali for providing a great deal of suggestions and corrections during the preparation and completion of my thesis.

I would like to extend my appreciation to Professor T. Huang and Professor J. H. Matthys in the Department of Civil Engineering for their comments and suggestions for this study.

I especially thanks to Dr. Ronald A. Schachar for providing medical-based information on the eye anatomy and function.

Finally, I thank my mother, father, my sister and my brother for their support from my country, Vietnam. I also extend my appreciation to aunt's family, my cousins my relative and my friends here, in USA, without whom the completion of this thesis was not possible.

<div align="right">July 25, 2005</div>

ABSTRACT

NONLINEAR FINITE ELEMENT MODEL ANALYSIS OF HUMAN

ACCOMMODATION LENS

Publication No. _____

Tri Le, M.S.

The University of Texas at Arlington, 2005

Supervising Professor: Ali Abolmaali

The crystalline human lens is modeled by using the finite element software, ABAQUS/CAE Version 6.5-1 as an axisymmetric shell to study the optical power and displacement of anterior and posterior poles induced due to zonule traction. Several different element types were tested to obtain the optimum mesh. These elements were three and six-noded triangular hybrid and four-noded quadrilateral hybrid for modeling of the cortex and nucleus. Constant strain triangular and regular quadrilateral elements were examined for modeling the capsule. One dimensional two degree of freedom spring elements were used to model the anterior, posterior, and equatorial zonules. Six different lens profiles were selected to mathematically model the lens geometry, which included Lizak; Krueger A; Krueger B; Strenk A; Strenk B; and Trial lens. A displacement-based incremental loading history was applied to the equatorial zonule to

conduct geometric nonlinear analysis. The converged solution was obtained by coupling Hilbert L-2 norm and equating external work done to internal system strain energy. The converged and optimum solution was compared with analytical solution reported in literature and was selected to conduct a comprehensive parametric study.

To study the effect of relative movement, due to zonule traction, between the capsule and the cortex, and cortex and nucleus, contact elements were introduced in the interface between each two regions. A parametric study was conducted to study the effects of force and geometry related variables on the lens's optical power based on the aforementioned lens profiles, including the variation of their central and capsular thicknesses within their physiologically possible range. The position of the zonules was also varied for each profile. The force related variables were stiffness of: capsule; cortex; nucleus and zonules.

The complete analysis of the parametric study including the comparison between this study and those reported in the literature is presented. The findings are also compared with physiology of the lens.

TABLE OF CONTENTS

Appendix

LIST OF ILLUSTRATIONS

LIST OF TABLES

CHAPTER 1

INTRODUCTION

1.1 The Human Eye

The human eye is essentially a spherical shell with a diameter of approximately 22.3 mm. The shell is white and non-transparent and is called sclera. The scleral shell is strong because it is composed of cross-linked collagen fibers. At the front of the scleral shell is the transparent cornea. The cornea is made of the same collagen fibers as the scleral; however, the corneal collagen fibers are highly ordered which decreases scattering of light and makes the cornea transparent. Below the cornea is a fluid, which is called aqueous humor (Duke-Elder and Wybar, 1961; Hogan et al, 1971). The aqueous humor circulates at a very slow rate, 2 micro liters/min, and supplies nutrition to the cornea and the lens (Becker and Hetherington, 1970).

The lens is located behind and adjacent to the iris. The central opening of the iris is called the pupil. The pupil changes size in response to light. The lens is an oblate spheroid and is composed of ectoderm, the same embryological tissue from which skin, hair, and nails are derived. Like skin and hair the lens grows throughout life. However since the lens is enclosed in a capsule, it cannot shed and it grows like an onion and gets larger with age (Mann, 1969). The lens is transparent because of is ordered protein structure (Schachar and Solin, 1975), the uniformity of its lens fibers (Kuszak et al, 2004), its lack of many cellular organelles (Hogan et al, 1971), and its negligible

1

extracellular space (Hogan et al, 1971). The lens is supported by zonules. There are three sets of zonules anterior, equatorial and posterior (Farnsworth and Burke, 1979; Streeten, 1982a, 1982b).

Behind the lens is a transparent viscous gel called vitreous. The vitreous is attached to the central posterior part of the lens, the peripheral retina, the optic nerve and the macular (Hogan et al, 1971). The vitreous can form areas that coalesce which will appear visually as strings or spots and are called vitreous floaters.

The retina contains two types of photoreceptors, rods and cones. The rods are predominately located in the peripheral retina and are responsible for motion detection and night peripheral, and black and white vision. The cones are predominately located in the center of the retina, which is called the macular. The cones are responsible for day, sharp, and color vision. The photoreceptors are located on the posterior part of the retina; i.e., light passes through the retina to reach the photoreceptors. Upon light stimulation the photoreceptors send a neuro-chemical message to the brain via the optic nerve. Significant image processing is done at the retinal level and at other way stations before final processing occurs in the occipital lobe (Adler, 1950).

The cornea and the lens are the optical components of the eye and together they focus and image on the macular in a patient with normal vision (emmetropia) who does not require spectacles. The relative position of the anterior-posterior position of the macular in relationship to the point of focus of the corneal-lens optical system is genetically determined. If the eye is too long then the patient will be nearsighted (myopic); i.e., the image will be formed in front of the retina. Myopia is corrected with

spherical negative concave lenses. If the eye is too short the patient will be farsighted (hyperopic) and the image will be formed behind the retina. Hyperopia is corrected with spherical positive convex lenses (Duke-Elder and Abrams, 1970).

The cornea is the major refractive element of the eye because the refractive index change between air, $n = 1$ and the cornea, $n = 1.337$ is large while the refractive indices between the cornea, aqueous humor, $n_a = 1.336$, the lens $n_l = 1.42$ and the vitreous, $n_v = 1.336$ is relatively small (Duke- Elder and Abrams, 1970).

The cornea in most individuals is relatively spherical with a radius of curvature of 7.8 mm. If the cornea has an ellipsoidal shape, the orthogonal radii of the curvatures of the corneal surface will be different and the patient will have astigmatism. Astigmatism is corrected with astigmatic lenses. Patients can have astigmatism combined with either myopia or hyperopia, in which case spectacles that have both a spherical and astigmatic correction are used. (Duke- Elder and Abrams, 1970)

The lens is an oblate spheroid (Kuzak et al, 2004). Its dimensions change with age. During the first two decades of life the central thickness decreases while the equatorial diameter rapidly increases. From that time on central thickness and the equatorial diameter slowly increase. At birth the equatorial diameter is 1.5 times its central thickness of 4.0 mm. At the age of 40 the central thickness is 2.2 times its central thickness of 4.13 mm (Schachar, 2005).

The youthful eye can change focus, accommodate far to near within 0.35 sec (Alpern, 1969). At birth the eye can focus at 8 cm, which is 12.5 diopters (Duane, 1917). A diopter is the inverse of the focal length in meters. Accommodation declines

3

in a linear fashion at the approximate rate of 0.25 diopters/year, so that by the age of 50 the patient essentially has no focusing ability (Donders, 1864). By the mid-forties, the focusing ability, accommodative amplitude, has declined so that the near point is more remote than the patient's normal near working distance. When this occurs the patient has presbyopia and will require reading glasses or bifocals (Donders, 1864).

<u>1.2 History of the Mechanism of Accommodation</u>

The mechanism by which the eye can accommodate has been speculated upon for centuries. It was generally believed that all parts of the body including the eye were divinely created. Vision was believed to occur according to the emanation hypothesis in which light was emitted from the brain through the lens of the eye. The lens of the eye not only emitted light to illuminate objects, it also served as the photoreceptor for the eye. The lens was considered the essential organ of vision. Although Aristotle (384-322 B.C) believed that vision occurred by the emission of light from external objects his concepts were not accepted. It was not until Al-Hazen (965-1043 AD) who was born in Basra and lived in Cairo that it was realized that Aristotle was right. As a result of Al-Hazen's books on optics, *Opticae Thesaurus* and *De Luce*, this scientific foundation for vision was disseminated, especially in the Arabic world. As a result, Ibn Rushd (1126-98), an Arabian-Spaniard, made the correct deduction that the retina and not the lens was the photoreceptor for images formed in the eye. Interestingly this concept was not accepted in Europe until the time of Kepler (1571-1630) (Duke-Elder and Abrams, 1970).

Roger Bacon (1214-1294) was an Englishman, and a member of the Franciscan Religious Order. He was an Arabic Scholar and learned from reading works of Al-Hazen. He suggested the use of convex lenses to improve near vision and attributed presbyopia to an increase in moisture of the eye and to wrinkling of the cornea (Duke-Elder, 1970). The Renaissance was beginning. Scientific thought was taking hold.

Snell (1591-1626), the Dutch mathematician, deduced the laws of refraction of light. He proved that the sine of the angle of incidence and the sine of the angle of refraction are related by the refractive of indexes of each media as follows:

$$n_1 \cdot \sin(\text{angle of incidence}) = n_2 \cdot \sin(\text{angle of refraction})$$

where n_1=index of refraction of the media of the incident ray and n_2 = the index of refraction of the media of the refracted ray. For example:
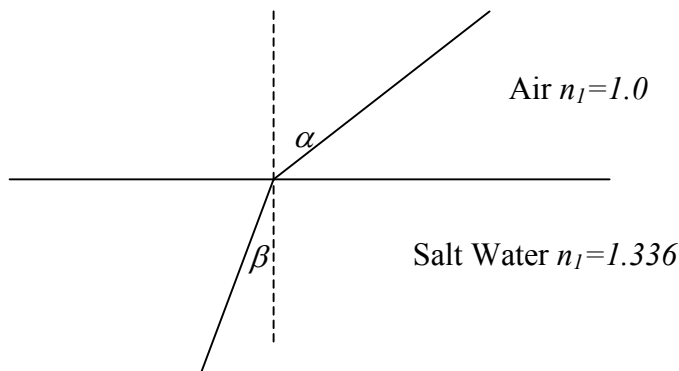
Figure 1.1 Refraction ray

the angle of refraction,

$$\beta = \sin^{-1}\left(\frac{n_1 \sin(\alpha)}{n_2}\right) = \sin^{-1}\left(\frac{\sin(45^0)}{1.336}\right) = 32^0$$

Optical physics was now on its way to significant advancement. However, how the eye worked was still a mystery (Duke-Elder, 1970).

A religious man, Scheiner (1575-1650) set out to determine if the eye followed the basic laws of optics (Scheiner, 1619). His simple ingenious experiment would change thinking about the eye forever. Scheiner asked the simple question: how can we confirm that the eye is an optical device? We see with our eyes, but how does the eye form an image? Does it work like a convex lens? (Duke-Elder and Abrams, 1970)

Optical lenses had been used for some time. Lens were probably first used by the Chinese as early as 2283 B.C. However, there is no authentic evidence that these early lenses were used for visual purposes. Generally, it is believed that they were used as sunglasses or to treat inflammations of the eye. The lenses were made of rock crystal, or quartz, or other transparent minerals many of which were colored. Emerald was a favorite crystal because of its transmission of green light, which was considered therapeutic. Inadvertently, it was noted that a convex shaped lens had magnifying power. A convex lens could be formed by water in a curved bottle. Technology moved forward.

Lenses could now be used to start a fire or to write extremely small hieroglyphics as documented in the 9th century B.C. It is believed that Nero in 54 A.D. was farsighted and used an emerald crystal to reduce glare and possibly correct his

hyperopia so that he could see at near. It was not until Roger Bacon (1214-1294) gave the Pope a reading glass that the idea of using a convex lens to improve near vision became common. In Venice in 1280, a city, which had developed significant technology for making glass, is credited with making the first true pair of spectacles in which lenses were held in a frame. The concept of correcting vision with spectacles spread throughout Europe. The relationship between external optics and vision was established. But how the eye focused and if it functioned like an optical system was still unknown (Duke Elder & Abrams, 1970).

Scheiner (1619) understood optics and performed the following experiment. He placed two adjacent vertical pinholes in a paper card. He made sure that the distance between the pinholes was very small so that the total outer boundary of both pinholes was less than the diameter of his pupil. He looked through both holes simultaneously and focused on a needle held perpendicular to the plane of the holes. When he focused on the needle, it appeared single; however, when he focused on a more distant object, the needle appeared doubled. Scheiner immediately knew the eye obeyed the laws of optics.

Figure 1.2 demonstrates the concepts used by Scheiner (1619) in his experiment. A convex lens focuses parallel rays of light at its focal point. Therefore, if a screen is placed at the focal point, a small spot of light will be seen on the screen. Just like when a magnifying glass is used to focus the light from the Sun to start a fire. The Sun is so far away that its rays of light are essentially parallel. The convex lens (magnifying glass) is moved toward and away from the object until the image of the

7

Sun on the object appears the smallest. The Sun's image appears as a very tiny spot of intense light. The distance that the lens is from the object, when the spot of light is the smallest, is the focal length of the lens. As the optical power of a convex lens is increased, its focal length becomes shorter and the spot size formed at its focal point becomes smaller. Conversely, as the optical power of a convex lens is decreased, it focal length increases and the spot size formed at its focal point becomes larger. The focal length is measured in meters and the shorter the focal length, the stronger the optical power of the lens. For convenience the inverse of the focal length in meters, diopters, are used so that the higher the dioptric power, the stronger the optical power of the lens (Ogle, 1968). For example, if a lens has a focal length of 0.5 meter, it will have an optical power of 2 diopters. That means if we want to start a fire with the Sun's rays, we would have to hold this lens 50cm from the object. On the other hand, if we have a lens with a focal length of 0.010 meters, it would have an optical power of 10 diopters and we would have to hold it 10 cm from the object to start a fire with the Sun's rays. The focal spot size of the 10 diopter lens is smaller than the focal spot formed by a 2 diopter lens. The 10 diopter lens is concentrating the Sun's parallel rays on a smaller spot and consequently the light intensity at the focal spot is much greater. Therefore, the focal spot formed by the 10 diopter lens will be much hotter and will start a fire easier and faster.

But what about the rays of light that are not parallel, which also pass through the lens? Only the rays of light that are parallel are brought to a focus on the screen that is placed at the focal length of the lens. The nonparallel rays pass through the convex

lens and begin converging; however, the screen is too close for them to come to a focus.

The nonparallel rays are spread around the central focal spot on the screen.
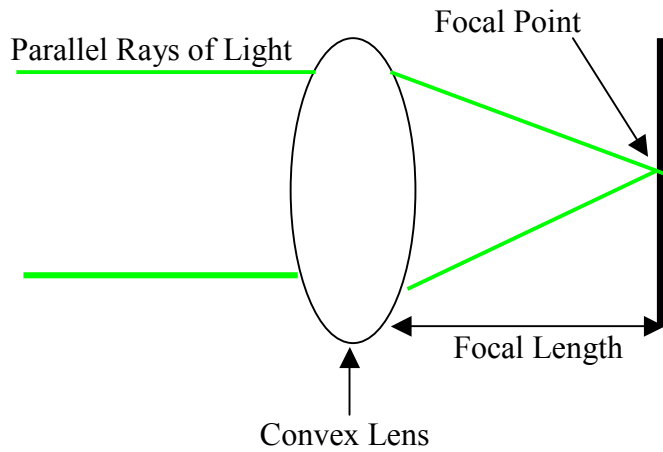
Figure 1.2 Focusing of parallel rays of light by a convex lens
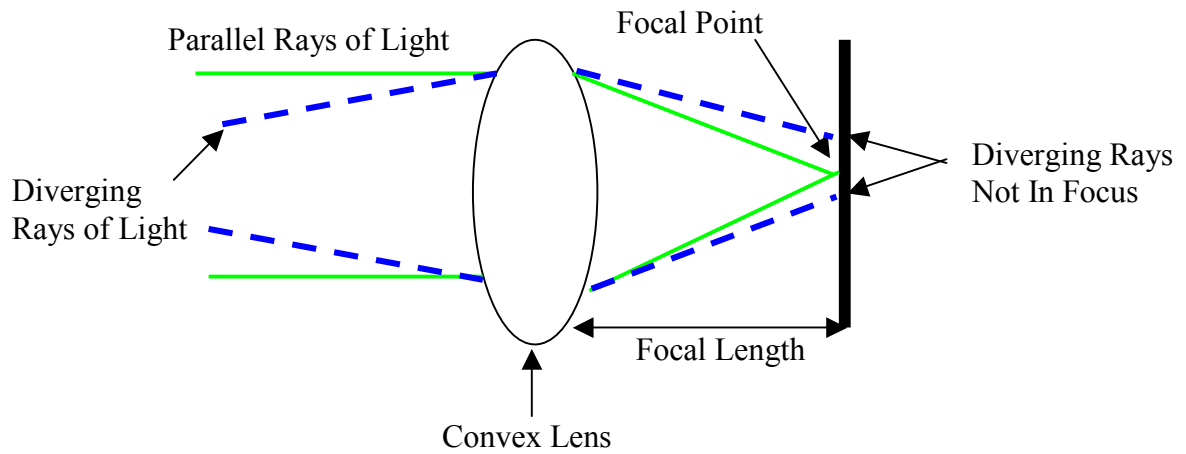
Figure 1.3 When the parallel rays of light from a distant object are in focus, the diverging rays of light from a near object are not in focus.

In order to bring the nonparallel rays in focus with the lens we have two options. We can move the lens away from the screen, or we can replace the lens with a stronger lens. By moving the lens away from the screen the diverging rays of light are brought into focus on the screen, but then parallel rays are out of focus as shown in Figure1.4.
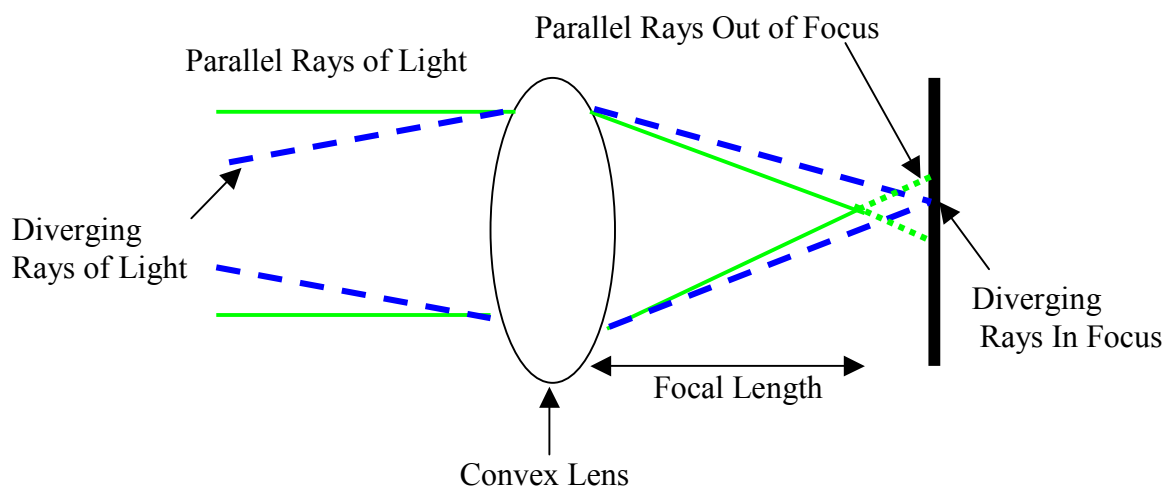
Figure 1.4 When the diverging rays of light from a near object are in focus the parallel rays of light from a distant object are not in focus.

The point is that the diverging rays and parallel rays cannot be in focus at the same time. When the parallel rays are in focus, the diverging rays are not and when the diverging rays are in focus, the parallel rays are not. When Scheiner (1617) placed the card with the two holes in front of his eye, he isolated the diverging and parallel rays as shown in the figure below.

Parallel Rays Out of Focus

Parallel Rays of Light

Diverging
Rays of Light

Card With Two Holes

Convex Lens

Focal Length

Diverging
Rays In Focus
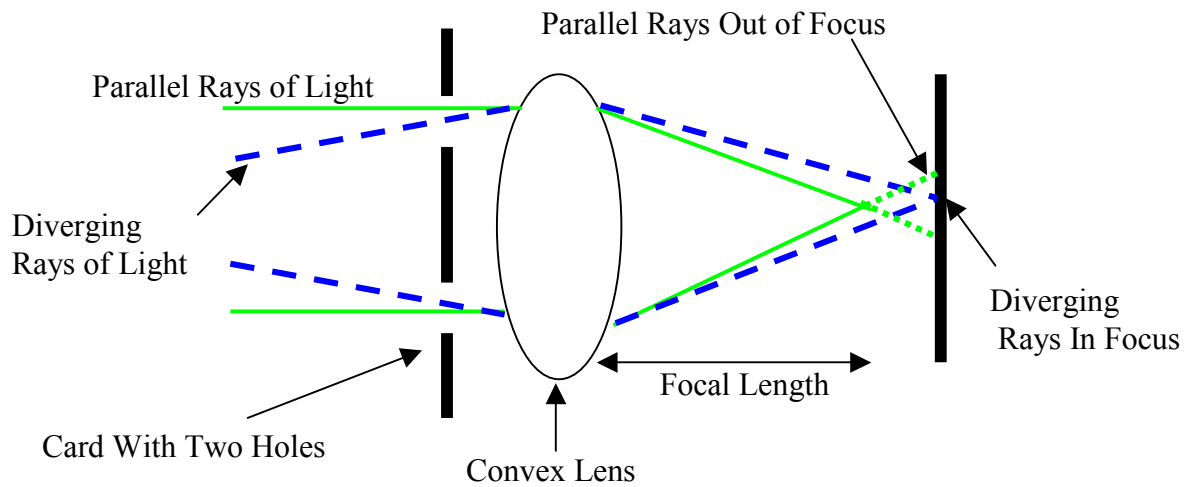
Figure 1.5 Scheiner's experiment showing with two holes in the card

When he looked at a distance object (parallel rays) it was in focus, but then the needle close to his eye (diverging rays) was out of focus and appeared double. The out of focus needle appeared double because each diverging ray that passed through the hole in the card formed a blurred image of the needle on his retina. Since there were two holes, there were two blurred images of the needle. Conversely when he focused on the needle, the distant object was blurred and appeared doubled. This proved that neither object was in focus at the same time. Therefore the optical system of the eye was changing focus. It responded just like the convex lens. We had to move the convex lens away to focus the diverging rays (near object) or toward the screen in order to focus the parallel rays (distance object) on the screen. The eye obeys the laws of physics. The eye is not able to focus on near and far objects simultaneously, it changes focus to see

objects at near and far. But how does it change its focus? This is where Scheiner (1617) left off.

The great German mathematician, Kepler (1571-1630) was responsible for proving that Mars rotated around the Sun in an ellipse, and definitely proving Copernicus's heliocentric theory. Kepler had smallpox at 4 years old which permanently impaired his vision. So it is understandable that he was interested in optics and the eye. In his classic work the Dioptrice (Kepler, 1611) he detailed the phenomenon of refraction of light and independently essentially discovered Snell's law of refraction. He developed the laws for the refraction of light by convex and concave lenses. He showed that the pupil of the eye did not act like a pinhole camera to focus light on the retina. He proved that the cornea and lens served as refracting elements to focus light on the retina (Duke-Elder and Abrams, 1970). From this time forward everyone was concerned with the dioptrics of the eye; i.e. the refraction of light by the eye. The word dioptrics is derived from the Greek words: dia meaning through, and optos meaning visible (Thomas, 1977).

Kepler (1611), in addition to describing the optics of the eye was very interested in how the eye focused. From his understanding of the refractive power of the lens and cornea he believed that the eye focused by forward and backward movement of the lens (Duke-Elder, 1970). This concept appeared straightforward. From the general understanding of the focal point of a convex lens, as discussed earlier, it seemed that this was the most likely mechanism by which the eye accommodated and was widely accepted by many authorities including Scheiner. The great French philosopher, René

12

Descartes (1596-1650) dissented, he believed, but did not prove, that the lens changed shape during accommodation and that it did not move anteriorly or posteriorly (Duke-Elder, 1970). He drew a diagram of how the lens could change shape so the eye could see at near and far (Descartes, 1677). He postulated that the surfaces of the lens would become steeper to see at near and flatter to see at distance. The debate on the mechanism of accommodation was just beginning.

von Haller (1708-1777) the founder of modern physiology and who was a Swiss anatomist believed that a decrease in pupil size allowed the eye to focus. He like Schiener noted that the pupil decreased in size during accommodation. Von Haller assumed that the smaller pupil size increased the depth of field so that no other focusing mechanism was required to see at near (Duke-Elder and Abrams, 1970). This concept was definitely disproved by both von Graefe (1860) and Hjort (1876) who observed full accommodative amplitudes in patients without an iris (Landolt, 1886).

Sturm (1697) studied astigmatism in an attempt to disapprove that the eye accommodated. In his work he discovered that with astigmatism there were two focal points as a result of the two different curvatures of the astigmatic cornea. Think of an American football, which has two orthogonal radii of curvatures. One radius is steeper than the other. The astigmatic cornea similarly has two orthogonal radii of curvatures so that there are two focal points, one for each radius. The distance between these two focal points is called the interval of Sturm. Sturm assumed that the eye focused by making use of these two different focal points. The problem with his theory is that most

people have minor astigmatism of < 1.50 diopters, which cannot account for the 10 diopters of accommodative amplitude of the young eye (Duke-Elder, 1970).

von Arlt (1812-1887) discovered that myopia occurred as a result of the elongation of the eye. He assumed that the extraocular muscles pulled the eye against the back of the orbit to shorten its length for distance vision, and that the extraocular muscle relaxed in near vision so the eye was elongated to focus on near objects (Tscherning, 1904).

Thomas Young (1773-1829), an Englishman, was a genius. At the age of two he was reading and by 14 years of age he mastered, Latin, Greek, Hebrew, Chaldec, Arabic, Syriac, Persian, French, Italian and Spanish. He was a physician and a physicist. He discovered interference with his famous double slit experiments which demonstrated that light acts like a wave. He made important contributions in all fields of science including physics, biology, zoology, hydrodynamics engineering and music. For example, he discovered capillarity, the relation of mass and velocity to work, that the stiffness of an object could be described by a constant, Young's modulus of elasticity, and that mortality could be predicted statistically. Young was the first to decipher hieroglyphics by translating the Rosetta Stone. All this was not enough; he fundamentally changed the understanding of accommodation and visual perception. He deduced that there were only three types of photoreceptors in the eye: Red, Green and Blue. With these three colored receptors we are able to see the entire color spectrum. His correct analysis of color vision is the basis for color film, color television, colored LCD, etc. But he did more; he proved that Descartes was correct. A change in

crystalline lens curvature is the basis for accommodation (Duke-Elder and Abrams, 1970).

Young's (1801) first objective was to determine if the eye elongated during accommodation and shortened with distance vision as a result of extraocular muscle contraction as Arlt suggested. Young knew that indentation of the posterior sclera applied pressure to the underlying retina. The pressure on the retina produces a sensation of seeing light at the point of scleral indentation. The sensation of light is called an entopic phenomenon (Duke-Elder et al, 1968). If the sclera is indented over the retina with a ring, then the entopic image will appear as a ring of light. Young realized that the greater the indentation of the sclera the larger the size of the entopic ring of light, and the less the scleral indentation the smaller the size of the entopic ring of light. With this basic understanding, Young had a method for determining the change in axial length of the eye during accommodation.

Young had very prominent eyes. Without anesthesia, it had not been discovered at that time, he placed a caliper that had rings attached to each side, around his eye. With his eye rotated nasally, he placed one ring on his cornea and the other over his macula. As he changed his point of focus, the entopic ring did not change size. This proved definitely that the eye does not elongate during accommodation.

Young (1801) next proved that the cornea does not move forward during accommodation. He placed a front surface mirror engraved with a scale at the side of his nose so that he could observe the front of his cornea while simultaneously focusing

15

on and object at different distances. He did not observe any movement of his cornea as he changed focus.

He next proved that the cornea does not change curvature during accommodation. He attached a convex lens possessing the optical power of the cornea to the bottom of eyecup filled with salt water and placed it over his cornea. The salt water in contact with the cornea eliminated the refractive power of the cornea; yet, he was still able to fully accommodate. Proving that the cornea was not involved in the focusing mechanism of the eye. It is interesting to not that this experiment was the basis for our present day contact lenses.

Young proved that the cornea does not play a role in accommodation. The next question was is the lens necessary for accommodation. He examined patients who did not have a crystalline lens, aphakes, either because of trauma or because the lens was removed surgically. He found that these patients could not accommodate. The lens was responsible for accommodation. But how did it work? Did it move forward and backward as Kepler (1611) hypothesized or did it change shape as Descartes (1677) suggested. He calculated how far the lens would have to move forward for 10 diopters of accommodation. He found it would have to move forward 10mm, a physical impossibility. The front of the lens is approximately 3 mm from the back of the cornea. That meant the lens had to change shape. But how could he prove that the lens changed shape during accommodation.

Young (1801) examined the change in shadows of parallel wires with accommodation. In distance gaze the shadows were perfectly straight, but with

accommodation, the peripheral shadows became outwardly convex. He noted that the outward convexity of the shadows was more easily observed with a larger pupil. He concluded that the central lens surface was steepening and the peripheral lens surface was flattening. To make sure that the peripheral flattening was not due to an artifact induced by the cornea, Young (1801) placed the eyecup filled with salt water on his eye to eliminate the cornea as a refractive element. He still observed the outward bowing of the peripheral shadows during accommodation while viewing through the eyecup.

Young had proven that the lens changes shape during accommodation by steepening centrally and flattening peripherally. Young saw the zonules supporting the lens and thought they were blood vessels. The ciliary muscle had not been discovered at that time. Young incorrectly surmised that the lens was muscular and contracted on its own during accommodation and received its nutrition via the zonules.

Purkinje (1823) noted that light from a candle was reflected from the front surface of the cornea and also from the anterior and posterior surfaces of the lens. When the image of an object is reflected from a convex surface, its size is dependent on the radius of curvature of the reflecting surface. The steeper the reflecting surface, the smaller the radius of curvature and the smaller is the size of the reflected image. Conversely, the flatter the reflecting convex surface, the larger the radius of curvature, and the larger is the size of the reflected image (Ogle, 1968). Using a magnifying glass and the light from a candle, Langenbeck (1849) observed that the reflected image of the candle from the central anterior surface of the lens decreased in size as a patient

accommodated. He concluded that Young and Descartes were correct; accommodation was due to a steepening of the central anterior surface of the lens.

Cramer (1851, 1853) confirmed Langenbeck's observation by using a modified telescope to accurately observe the changes of the reflections (Purkinje images) from the anterior surface of the lens. He noted that the anterior surface of the crystalline becomes more convex, but the posterior surface did not appear to change shape.

Helmholtz (1821-1894) improved Cramers' telescope by placing crossed glass plates between the patient's eye and the telescope, so that the reflections from the anterior and posterior lenses surfaces were doubled (Helmholtz, 1855). This permitted accurate determination of the change in size of the reflected images. He noted that the reflections from both the anterior and posterior lens surfaces decreased in size during accommodation. He also noticed that the reflections moved apart. That meant that both lens surfaces were becoming steeper, more convex, and the central lens thickness was increasing during accommodation.

Just prior to Cramer and Helmhotz' experiments the ciliary muscle was identified Brucke, (1846) and Bowman (1849). With knowledge of the existence of the circular ciliary muscle, Helmholtz (1855) postulated that during accommodation the circular ciliary muscle contracted and decreased its internal diameter. The reduction of the internal diameter of the ciliary muscle decreased tension on the zonules so that the lens could roundup under the influence of its own elasticity. During distance vision the ciliary muscle would relax and its internal diameter would increase so that there was increased tension on the zonules and the lens would flatten and thin during distance

vision. Helmholtz postulated that an age-related stiffening of the lens was the etiology of presbyopia.

Tscherning (1862-1930) re-examined Young's observations and confirmed that the peripheral anterior surface of the lens flattened during accommodation (Tscherning, 1901). He placed two lights so they reflected from the peripheral anterior surface of the lens and another two lights so they reflected from the center of anterior surface of the lens. When the patient accommodated, the reflections from the central anterior surface of the lens moved closer together while the reflections from anterior peripheral surfaces moved apart. This confirmed that the central anterior surface of the lens was steepening while the peripheral anterior surface of the lens was flattening. Young was right, the spherical aberration of the lens decreases during accommodation as a result of peripheral surface flattening.

Tscherning (1901) postulated that the ciliary muscle applied increased tension to the zonules and pulled the lens against the anterior vitreous. He thought that the resistance of the vitreous caused the lens to move forward and bulge during accommodation. He did not accept Helmholtz's central thickness measurements, and postulated that central lens thickness decreased or stayed the same during accommodation. Tscherning attributed presbyopia to enlargement of the lens nucleus.

Helmholtz's theory is not consistent with anterior surface peripheral flattening that occurs during accommodation. According to Helmholtz's theory the lens should round up and both the central and peripheral surfaces should simultaneously steepen during accommodation. As a result of this and other inconsistencies in Helmholtz's

theory multiple variations of his theory have been postulated (Gull Strand, 1911; Fincham, 1937; Weale, 1982; Farnsworth and Shyne SE; Rohen, 1979; Tamm, et al, 1992; Coleman and Fish, 2001; Strenk et al, 2005; Sarfarazi 2005), all of which are based on relaxation of the zonules during accommodation. For example, Fincham (1893-1963) noted that the lens capsule was thicker in the periphery than at the center of the lens. Fincham (1937) attributed the peripheral surface flattening that occurs during accommodation to the variation in capsular thickness. These theories attribute presbyopia to stiffening of the crystalline lens stroma, or capsule atrophy of the ciliary muscle, or stiffening of the ciliary muscle attachments.

Schachar (1992) has proposed an alternate mechanism for accommodation. In his theory the equatorial zonules are the active component of accommodation. According to him, equatorial zonular tension increases during accommodation while the anterior and posterior zonules relax. The increased equatorial zonular tension results in central lenticular surface steepening, peripheral surface flattening, an increase in central thickness, and an increase in central optical power. He attributes presbyopia to normal equatorial lens growth (Schachar, 1992, 1994, 1996, 1999, 2001, 2001, 2002a, 2002b, 2005b)

1.3 The History of the Finite Element Method (FEM)

Archimedes (287 BC to 212 BC) was the first to conceive of the finite element method (FEM) to determine that the center of gravity of any parallelogram lies on the line joining the middle points of the opposite sides of the parallelogram. In order to make this deduction he divided the parallelogram into multiple smaller parallelograms-

elements (Dugas, 1988). The finite element method was born. However, it was very slow to develop because the required calculations to apply the method were too extensive. Once fast inexpensive computers became available, the large number of calculations required for the finite element method could be preformed reliably and rapidly.

The modern finite element method begins in the early 1900's when theoretical engineers approximated and modeled elastic continua using discrete equivalent elastic bars (Hrennikoff A. 1941). However, it was Courant (1888-1972), the famous mathematician, who really developed the finite element method when he investigated torsion problems by using piecewise polynomial interpolation over triangular subregions (Courant, 1943).

Boeing initially applied the finite element method, calling it the "Direct Stiffness Method," to design airplane wings (Levy 1953). However, it was Clough (1960, 1963, 2004) who coined the name "Finite Element Method." He established the finite element method by demonstrating that he could obtain agreement between his finite element method of the stresses in a vibrating wing and laboratory physical measurements. He noted that the calculated results converged toward the physical model when the triangular mesh elements of the finite element model were refined. (Clough, 1960, 1963, 1965, 2004). In 1992 Wilson, Clough's graduate student, applied computer techniques to make the finite element reliable and applicable to multiple problems (Wilson, 1993). As a direct result of Clough's demonstration of the reliability of the finite element method (Clough, 2004), it was applied to all areas of engineering

including civil, mechanical, electrical and hydrodynamics (Zienkiewicz and Cheung, 1967; Zienkiewicz, 1979, Patankar, 1991).

CHAPTER 2

FINITE ELEMENT MODEL

2.1 Introduction

This chapter discusses the finite element modeling of human crystalline lens using axisymmetric elements. The lens capsule, cortex and nucleus are modeled by employing ABAQUS software. Several types of triangular and quadrilateral elements including: three node, three node hybrid, six node, and six node hybrid triangular; and four node, four node hybrid, eight node, and eight node hybrid quadrilateral elements, were evaluated for modeling the lens. Each of the elements with the ABAQUS sign designation is shown in Table 2.1. The optimum mesh with regard to element type was selected and the analysis was performed to include geometric and contact nonlinearities. A coupled energy based and norm two (II.II) based convergence criteria were used to obtain the converged solution.

2.2 Lens Geometry and Property

2.2.1 Lens Geometry

The crystalline lens is located behind the iris and therefore its complete shape *in vivo* cannot be determined biomicroscopically. For this reason profile photographs of the lens (Scheimpflug photographs) only reveal approximately three fourths of the *in vivo* lens profile. In previous mathematical modeling the entire lens shape was

estimated by combining the partial lens profiles obtained from Scheimpflug photographs with *in vitro* histological measurements of the total lens.

With the advent of magnetic resonance imaging (MRI) the entire profile of the human crystalline lens is visible *in vivo*. However, the resolution of the clinical MRI is presently only approximately 150 microns. Therefore, even profiles of the lens obtained with MRI are estimates of the exact lens shape. For example, it has been demonstrated, by optical measurements, using reflections from the lens surface, that there is very little difference in the shape of the young adult lens; however, MRI profiles show significant variation. Therefore, in order to understand the response of the lens to an applied force, examination of multiple MRI profiles are required.

The human crystalline lens is an oblate spheroid and therefore is axisymmetric. The young adult lens has an equatorial diameter that is approximately twice its central thickness. The following formula for the lens surface introduced by Chien et al., (2003) was used.

$$y(x) = \left[b + c \left(\sin^{-1} \left(\frac{x}{a} \right) \right)^2 + d \left(\sin^{-1} \left(\frac{x}{a} \right) \right)^4 \right] \cdot \cos \left(\sin^{-1} \left(\frac{x}{a} \right) \right) \qquad (2.1)$$

This formula was developed by carefully outlining six lens profiles obtained from MRI images of a: 60y/o lens (Lizak); 40y/o (Krueger A); 40 y/o (Krueger B); 20 y/o (Strenk A); 20y/o (Strenk B); and Trial lens, which are shown in Figures 2.4, 2.5, 2.6, 2.7, 2.8 and 2.9 respectively. The lenses had central optical powers as calculated from the thick lens formula of 19.3 diopters, 20.7 diopters, 23.5 diopters, 21.2 diopters, 29.0 and 18.0 diopters respectively.

The formula which for the lens profiles has the following characteristics: it is a continuous function in which the radii of curvatures at any point on the lens surface are smoothly varied, the radii do not change abruptly at the optical axis, the radii are identical at the equator where the anterior and posterior surfaces meet, and they have a positive Guassian curvature everywhere on the surface. For these reasons this formula was used for the FEM models of each lens.

The lens is enclosed within a capsule. The thickness of the capsule varies around the lens. The variation of the capsular thickness was incorporated into the FEM model by using the formulas given by Equation 2.1.

The lens stroma consists of an outer cortex and an inner central nucleus. Based on *in vivo* Scheimpflug photographs (Dubbelman et al, 2003), the thickness of the central nucleus was estimated as a percentage of the central thickness of the entire lens. The offset of the equatorial plane of the nucleus from the equatorial plane of the entire lens was estimated from histological photographs (Hogan et al. 1971) as presented in Figures 2.1 and 2.2. For the lens stroma the nucleus and cortex were considered as one unit with a common elastic modulus as shown in Figure 2.3.
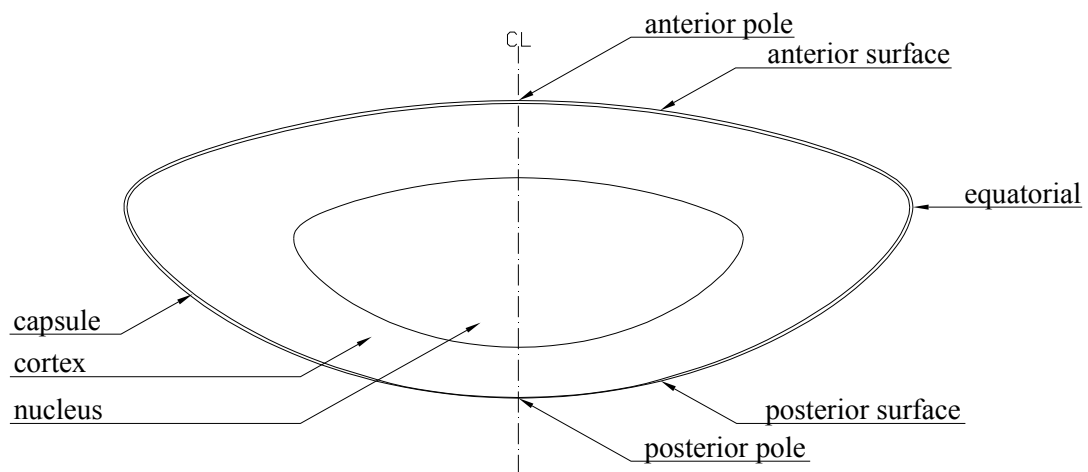
Figure 2.1 The geometry of the crystalline lens
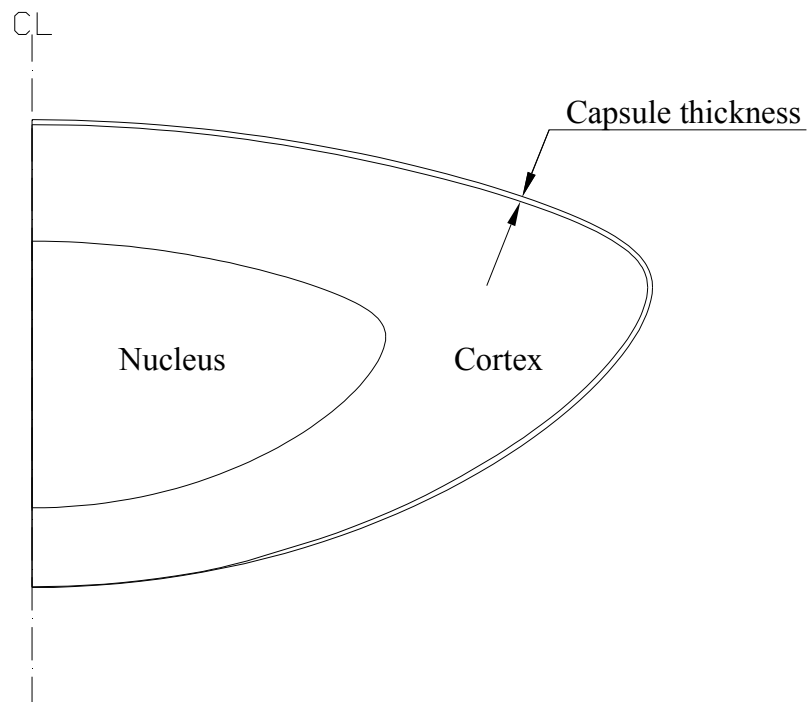
Figure 2.2 The crystalline lens model – with its cortex and nucleus
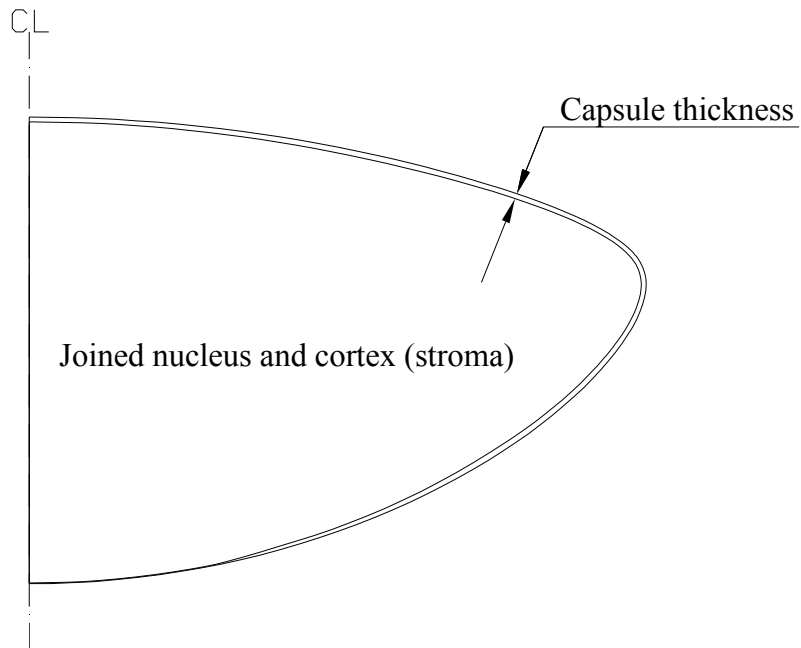
Figure 2.3 The crystalline lens with the cortex and nucleus treated as one unit.
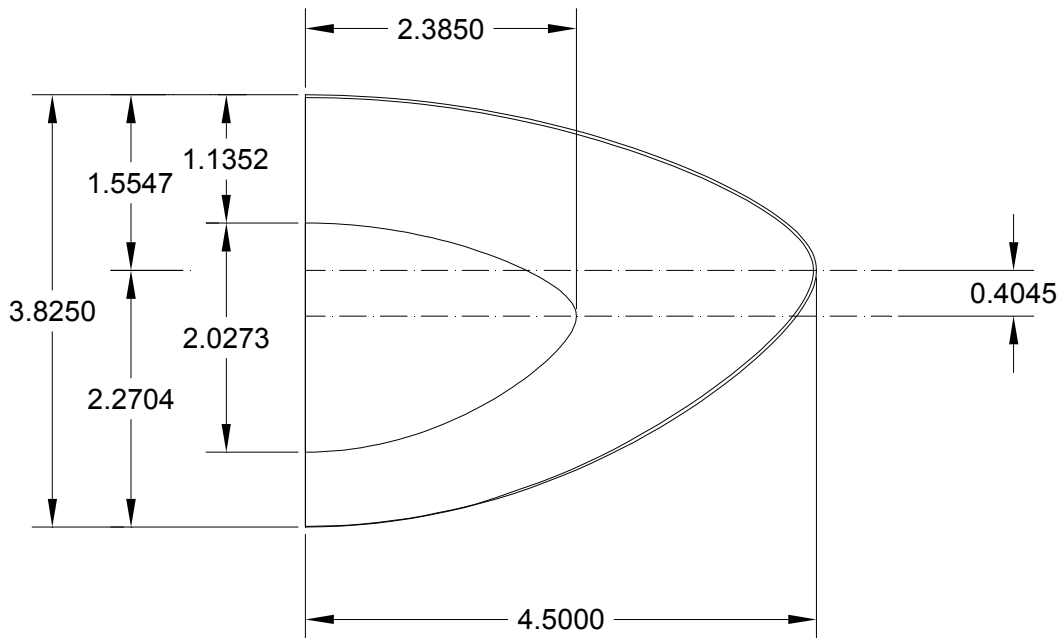
Figure 2.4 The crystalline lens model – Lizak profile
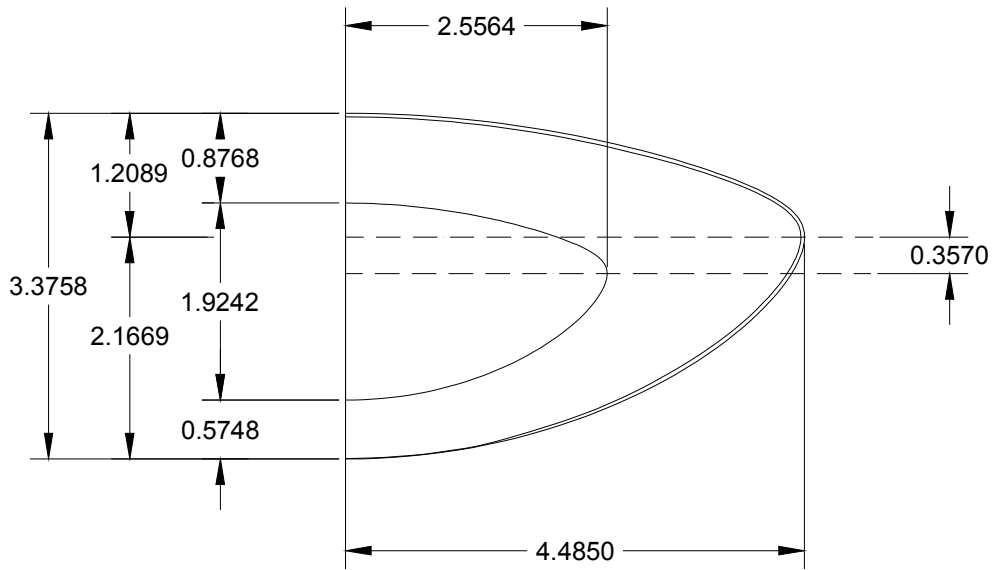
Figure 2.5 The crystalline lens model – Krueger profile A
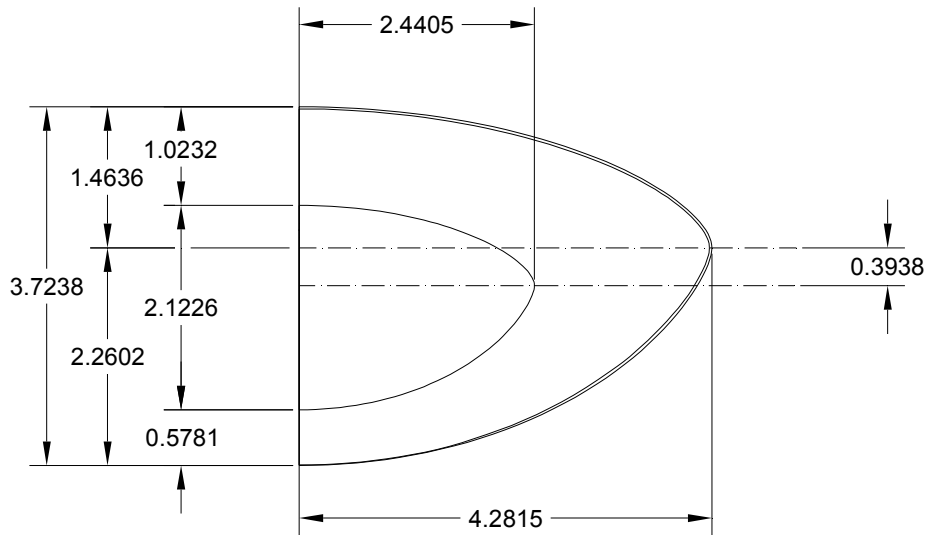
Figure 2.6 The crystalline lens model – Krueger profile B

28
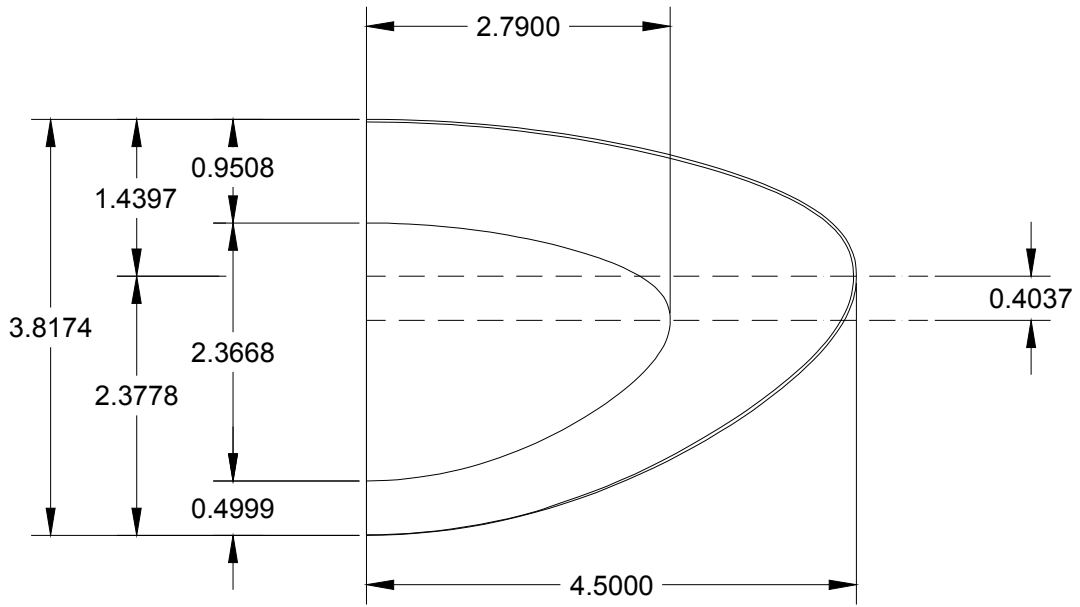
Figure 2.7 The crystalline lens model – Strenk profile A
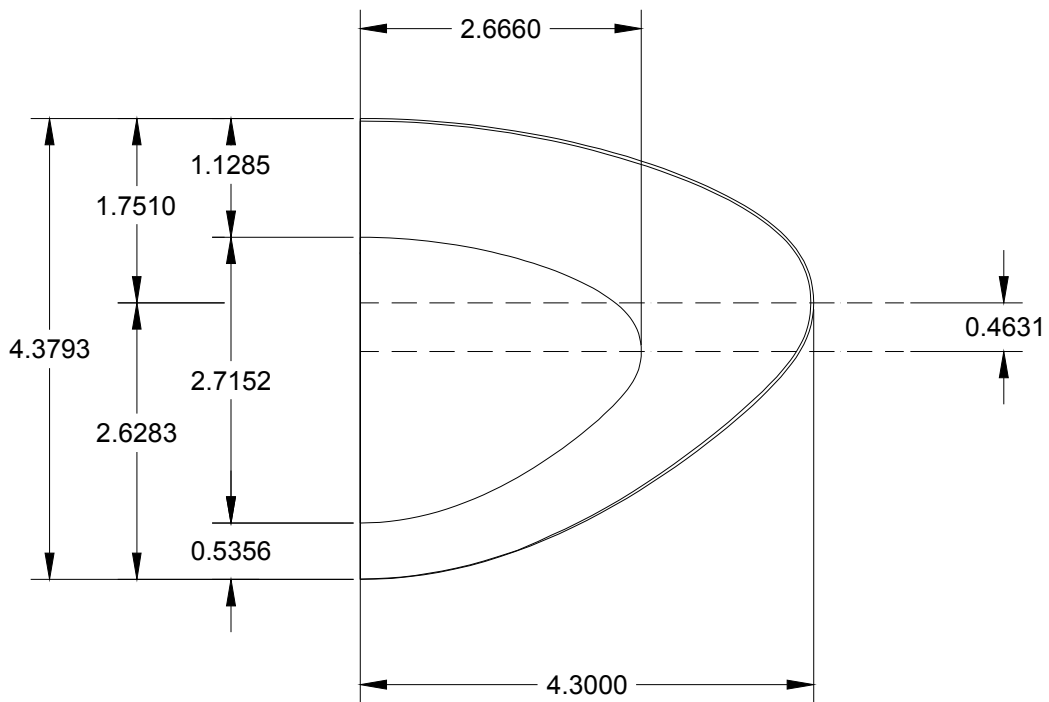
Figure 2.8 The crystalline lens model – Strenk profile B

29
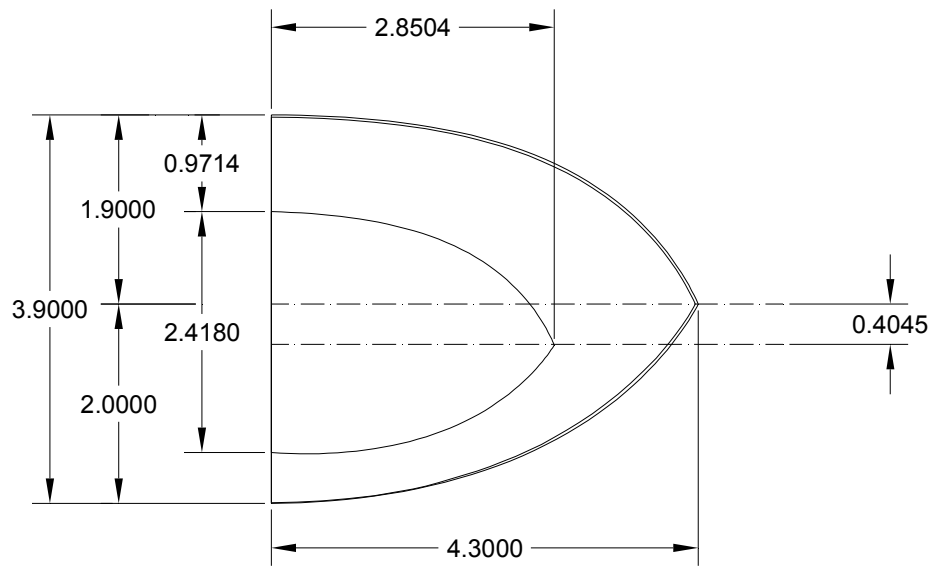
Figure 2.9 The crystalline lens model – Trial lens

2.2.2 Material Properties

The lens capsule is thin with an average thickness of 20 microns. The central posterior capsule has a constant thickness throughout life. The rest of the capsule continues to thicken throughout life, reaching a maximum of about 35 microns at 80 years of age (Krag and Andreassen, 2003). It has a Poisson's ratio of 0.47 (Fisher, 1971). The elastic modulus of the posterior capsule is 0.75 MPa and remains constant throughout life. The elastic modulus of the anterior capsule at birth is approximately 0.75 MPa and then increases to 1.5 MPa at 35 years of age and then remains constant with increasing age (Krag and Andreassen, 2003).

The lens is nearly incompressible with a bulk modulus that is higher than water. Using non-invasive Brillouin light scattering the bulk modulus of the lens cortex is 2.8

GPa and 3.7 GPa for the nucleus (Subbaram et al. 2002). The Poisson's ratio of the lens stroma is 0.49999999. This Poisson's ratio can be calculated from the measured shear of the young lens (Heys et al. 2004), which is less than or equal to 50 Pa, and the measured bulk modulus of 2.8 GPa.

The ciliary muscle applies the force, which is transduced to the lens capsule by the zonules. The reported elastic modulus of the zonules is 1.5 MPa (van Alphen and Graebel, 1991).

Because there is an interface between the lens capsule and the cortex, and between the cortex and nucleus, the effect of placement of contacts between these interfaces is evaluated.

2.3 Axisymmetric Finite Element

Axisymmetrical problems are associated with bodies of revolution; the z-axis is the axis of revolution or axis of symmetry. The two displacements are $u(r,z)$ in the r and z directions respectively. All of the parameters such as elastic constants, body forces, surface tractions are assumed to depend on r, z only. Examples of two typical axisymmetric problems are shown in Figure 2.10.

The stress-strain relation can be expressed as

$$\{\sigma\} = [C]\{\varepsilon\}$$

31

$$
\begin{Bmatrix} \sigma_r \\ \sigma_\theta \\ \sigma_z \\ \tau_{rz} \end{Bmatrix} = \frac{E(1-v)}{(1+v)(1-2v)} \begin{bmatrix} 1 & \dfrac{v}{(1-v)} & \dfrac{v}{(1-v)} & 0 \\[2mm] \dfrac{v}{(1-v)} & 1 & \dfrac{v}{(1-v)} & 0 \\[2mm] \dfrac{v}{(1-v)} & \dfrac{v}{(1-v)} & 1 & 0 \\[2mm] 0 & 0 & 0 & \dfrac{(1-2v)}{2(1-v)} \end{bmatrix} \cdot \begin{Bmatrix} \dfrac{\partial u}{\partial r} \\[2mm] \dfrac{u}{r} \\[2mm] \dfrac{\partial w}{\partial z} \\[2mm] \dfrac{\partial u}{\partial z} + \dfrac{\partial w}{\partial r} \end{Bmatrix} \tag{2.2}
$$

(a)

(b)
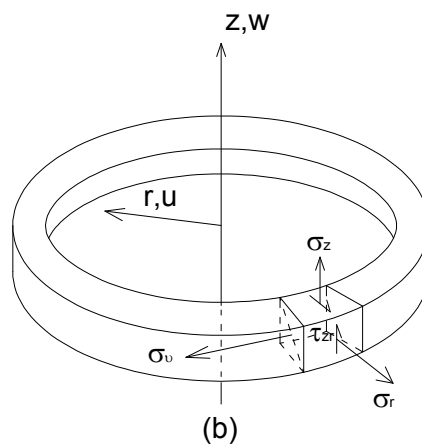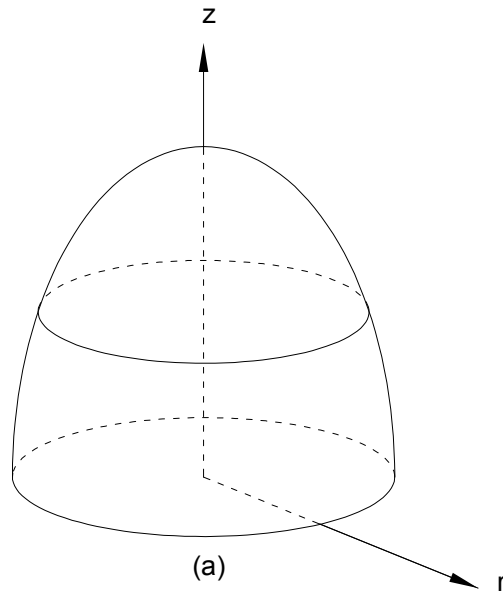
Figure 2.10 Examples of two typical axisymmetric problems. (a) Cone shape (b) Ring shape.

The lens is modeled and analyzed using an FEM software program (ABAQUS/CAE Version 6.5-1). The lens capsule, cortex, and nucleus are each modeled as closed axisymmetrical shells. The shell elements and the types of elements used for modeling are presented in Table 2.1. The capsule and the lens are assumed to be homogeneous and orthotropic.

Because the crystalline lens is axisymmetrical, only a two-dimensional profile is required. The two dimensional profile of the lens must include the major equatorial axis and the minor anterior-posterior axis.

2.4 Type of Element Used

Three node triangular elements are commonly used in FEM analysis because they are easy to generate. However, for most of problem, quadrilateral elements give more accurate results with a coarser mesh (Blacker and Stephenson, 1991; Talbert and Parkinson, 1990). In addition, triangular elements are not as good a choice because triangular elements have less degree of freedom than quadrilateral elements, thus many more triangular elements (finer mesh) are required elements to obtain a converged result. The typical converged quadrilateral mesh is shown in Figures 2.10.

The ABAQUS element types and corresponding element number used during different modeling stages and the parametric study of Chapter 3 are shown in the Table 2.1. The hybrid elements presented in this table (i.e., CAX3H, CAX6H, CAX4H, and CAX8H) are used to model the nearly incompressible regions of the cortex and nucleus.
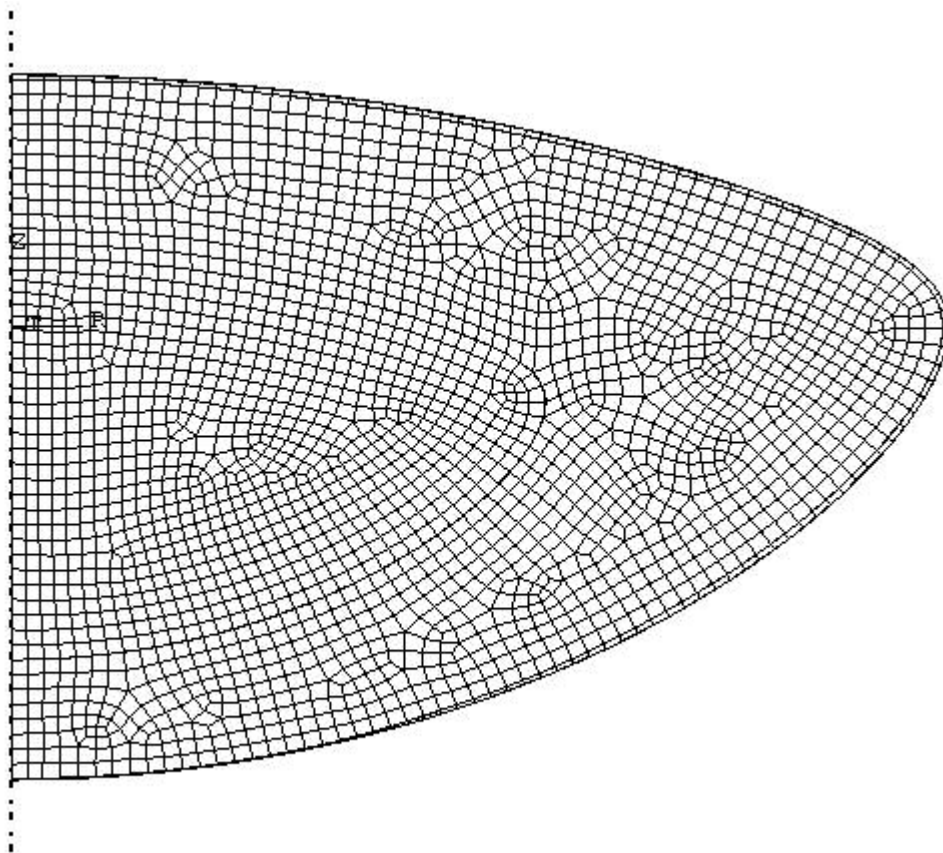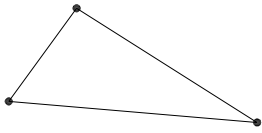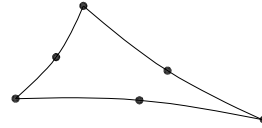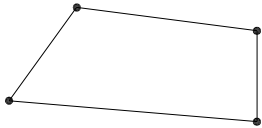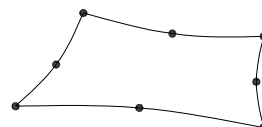
Figure 2.11 The crystalline lens model – quadrilateral typical mesh

Table 2.1 Element types and corresponding element number

Axisymmetric element (in ABAQUS)	Description	D.O.F	Element shape
CAX3	3 nodes element	6	
CAX3H	3 nodes hybrid element	6	
CAX6	6 nodes element	12	
CAX6H	6 nodes hybrid element	12	
CAX4	4 nodes element	8	
CAX4H	4 node hybrids element	8	
CAX8	8 node element	16	
CAX8H	8 nodes hybrid element	16	

2.5 Description of Hybrid Elements

As discussed previously the lens stroma, including its cortex and nucleus, is nearly incompressible because it has a Poisson's ratio > 0.4999999 and a bulk modulus that is much greater than its shear modulus.

There are many problems that involve the prediction of the response of an almost incompressible material. This is especially true at large strains, since most solid materials show relatively incompressible behavior under large deformations. When the material response is incompressible, the solution to a problem cannot be obtained in terms of displacement only, since a purely hydrostatic pressure can be added without changing the displacement. Conversely, a very small change in displacement can

produce a large change in hydrostatic pressure. Consequently, a pure displacement-based solution is too sensitive to be numerically useful; e.g., numerical computational rounding may cause the method to fail. This is manifested in the analysis by volume strain "locking" which can even occur even with smaller Poisson's ratio, v, of the order of $v = 0.49$. To overcome this singularity behavior in the system, the stress induced in response to pressure is treated as an independently interpolated basic solution variable. Using a Lagrange multiplier, this pressure-stress variable is coupled to the displacement solution using constitutive theory and a compatibility condition. This independent interpolation of the pressure-stress variable is the basic formulation of a "hybrid" FEM mesh element. More precisely, the hybrid mesh element uses a "mixed formulation" of the displacement and stress variables with an augmented variational principle to approximate the equilibrium equation and compatibility conditions.

The formulation for the hybrid element taken directly from Theory Manual is presented as follows:

The internal virtual work is:

$$\delta \mathbf{W} = \int_V \boldsymbol{\sigma} : \delta \varepsilon \, dV \tag{2.3}$$

where $\delta \varepsilon = symm\left(\dfrac{\partial \delta \mathbf{u}}{\partial \mathbf{x}} \right)$ (2.4)

where $\delta \mathbf{u}$ is the virtual displacement field;

$\boldsymbol{\sigma}$ is the true Cauchy stress;

V is the current volume;

$\delta \mathbf{W}$ is the virtual work as define by equation.

36

In a displacement based formulation the Cauchy stress, σ, is obtained with the constitutive equations from the deformation, usually in rate form:

$$d\boldsymbol{\sigma} = \mathbf{C}:d\boldsymbol{\varepsilon} + d\mathbf{W}.\boldsymbol{\sigma} - \boldsymbol{\sigma}.d\mathbf{W} \qquad (2.5)$$

where $\mathbf{C}$ is the material stiffness matrix and $d\mathbf{W}$ is the rate of rotation of material.

The Cauchy stress is modified by introducing and an independent hydrostatic pressure field $\hat{p}$ as follow

$$\bar{\boldsymbol{\sigma}} = \boldsymbol{\sigma} + (1-\rho)\mathbf{I}(p-\hat{p}) \qquad (2.6)$$

where

$p = -\dfrac{1}{3}trace(\boldsymbol{\sigma})$ is the hydrostatic pressure stress and ρ is a small number. If ρ was set equal to zero, the hydrostatic component in $\bar{\boldsymbol{\sigma}}$ would be identical to the independent pressure field $\hat{p}$, corresponding to a pure "mixed" formulation. The small nonzero value (10^{-9}) is chosen to avoid equation solver difficulties. This relation is used in incremental form:

$$\bar{\boldsymbol{\sigma}} = \bar{\boldsymbol{\sigma}}^0 + \Delta\boldsymbol{\sigma} + (1-\rho)\mathbf{I}(p-\hat{p}) \qquad (2.7)$$

Where $\bar{\boldsymbol{\sigma}}^0$ is the modified Cauchy stress at the start of the increment. The modified Cauchy stress is used in the virtual work expression and augments the expression with the Lagrange multiplier enforced constraint $\Delta p - \Delta\hat{p} = 0$:

$$\delta\overline{W} = \int_V [\bar{\boldsymbol{\sigma}}:\delta\varepsilon + \mathbf{J}^{-1}\delta\lambda(\Delta p - \Delta\hat{p})]dV \qquad (2.8)$$

With J the volume change ratio (Jacobian) and $\delta\lambda$ a Lagrange multiplier whose interpolation must still be determined. $\Delta\hat{p}$ will be interpolated over each element so that the constraint is satisfied in an integrated (average) sense. Since Δp is the value of the equivalent pressure stress increment computed from the kinematics solution, Equation 2.7. does not make sense if the material is fully incompressible because then Δp cannot be computed. For the purpose of development we regard the bulk modulus as finite, and we will be able to show that the final formulation approaches as a usable limit as we allow the bulk modulus to approach infinity.

For the formulation the tangent stiffness (the Jacobian), we need to dine the rate of change of $\delta\overline{\mathbf{W}}$. Therefore, we rewrite the virtual work equation in terms of the reference volume V^0:

$$\delta\overline{\mathbf{W}} = \int_{V^0}[\mathbf{J}\overline{\mathbf{\sigma}} : \delta\varepsilon + \delta\lambda(\Delta p - \Delta\hat{p})]dV^0 \qquad (2.9)$$

The rate of change

$$d\delta\overline{\mathbf{W}} = \int_{V^0}[d\mathbf{J}\overline{\mathbf{\sigma}} : \delta\varepsilon + \mathbf{J}d\overline{\mathbf{\sigma}} : \delta\varepsilon + \mathbf{J}d\overline{\mathbf{\sigma}} : \delta\varepsilon + \delta\lambda(dp - d\hat{p}) + d\delta\lambda(\Delta p - \Delta\hat{p})]dV^0 \qquad (2.10)$$

This expression is rewritten in term of the current volume:

$$d\delta\overline{\mathbf{W}} = \int_{V}[d\overline{\mathbf{\sigma}} : \delta\varepsilon + d\varepsilon : \mathbf{I}\overline{\mathbf{\sigma}} : \delta\varepsilon + \overline{\mathbf{\sigma}} : \delta\varepsilon + \mathbf{J}^{-1}\delta\lambda(dp - d\hat{p}) + \mathbf{J}^{-1}d\delta\lambda(\Delta p - \Delta\hat{p})]dV \quad (2.11)$$

where we used the identity $\mathbf{J}^{-1}dJ = \mathbf{I} : d\varepsilon$

The rate of the modified stress follows from Equation 2.7 and the constitutive equations:

$$d\overline{\mathbf{\sigma}} = \mathbf{C} : d\varepsilon + (1 - \rho)\mathbf{I}(dp - d\hat{p}) + d\mathbf{W}\overline{\mathbf{\sigma}} - \overline{\mathbf{\sigma}}d\mathbf{W} \qquad (2.12)$$

38

where $p = -\dfrac{1}{3} trace(\mathbf{\sigma}) = -\dfrac{1}{3}\mathbf{I} : \mathbf{C} : d\varepsilon$

and we used the fact that

$$d\mathbf{W} \cdot \overline{\mathbf{\sigma}} - \overline{\mathbf{\sigma}} \cdot d\mathbf{W} = d\mathbf{W} \cdot \mathbf{\sigma} - \mathbf{\sigma} \cdot d\mathbf{W} \qquad (2.13)$$

since $\overline{\mathbf{\sigma}}$ and $\mathbf{\sigma}$ differ only in the hydrostatic part. Substituting these expressions into the expression for the rate of virtual work yields

$$d\delta\overline{\mathbf{W}} = \int_V \Big\{ \delta\varepsilon : \mathbf{C} : d\varepsilon + \delta\varepsilon : \overline{\mathbf{\sigma}}\mathbf{I} : d\varepsilon - \frac{1}{3}(1-\rho)\delta\varepsilon : \mathbf{I} \cdot \mathbf{I} : \mathbf{C} : d\varepsilon$$

$$- (1-\rho)\delta\varepsilon : \mathbf{I}d\hat{p} - \frac{1}{3}\mathbf{J}^{-1}\delta\lambda\mathbf{I} : \mathbf{C} : d\varepsilon - \mathbf{J}^{-1}\delta\lambda d\hat{p} \qquad (2.14)$$

$$+ \mathbf{J}^{-1}d\delta\lambda(\Delta p - \Delta\hat{p}) + \overline{\sigma} : d\delta\varepsilon + \delta\varepsilon : (d\mathbf{W}\overline{\mathbf{\sigma}} - \overline{\mathbf{\sigma}}d\mathbf{W}\Big\}dV$$

It remains to choose $\delta\lambda$ to get a symmetric expression for the rate of virtual work, we choose

$$\delta\lambda = (1-\rho)\mathbf{J}\left(\frac{1}{3\mathbf{K}}\mathbf{I} : \mathbf{C} : \delta\varepsilon - \mathbf{I} : \delta\varepsilon + \frac{1}{\mathbf{K}}\delta\hat{p}\right) \qquad (2.15)$$

where

$$\mathbf{K} = \frac{1}{9}\mathbf{I} : \mathbf{C} : \mathbf{I}$$

is the bulk modulus. This is a suitable choice for $\delta\lambda$, because the term proportional to $\delta\hat{p}$ ensures that the modified incremental pressure field, $\Delta\hat{p}$, is properly constrained to the incremental pressure, Δp. If we assume that the volumetric moduli *I:C* and $\mathbf{K}$ change slowly with strain and ignore changes in volume, we can write for the second variation $d\delta\lambda$:

$$d\delta\lambda = (1-\rho)\mathbf{J}\left(\frac{1}{3\mathbf{K}}\mathbf{I}:\mathbf{C}-\mathbf{I}\right):d\delta\varepsilon \qquad (2.16)$$

Hence, we find for the virtual work expression

$$\delta\overline{\mathbf{W}} = \int_V\left[\tilde{\sigma}:\delta\varepsilon + (1-\rho)(\Delta p - \Delta\hat{p})\frac{1}{\mathbf{K}}\delta\hat{p}\right]dV \qquad (2.17)$$

where

$$\tilde{\sigma} = \overline{\sigma} + (1-\rho)(\Delta p - \Delta\hat{p})\left(\frac{1}{3\mathbf{K}}\mathbf{I}:\mathbf{C}-\mathbf{I}\right) \qquad (2.18)$$

For the rate of change of virtual work we find

$$d\delta\overline{\mathbf{W}} = \int_V\left\{\delta\varepsilon:\mathbf{C}:d\varepsilon - \frac{1}{9\mathbf{K}}(1-\rho)\delta\varepsilon:\mathbf{C}^T:\mathbf{II}:\mathbf{C}:d\varepsilon + \delta\varepsilon:\overline{\sigma}\mathbf{I}:d\varepsilon\right.$$

$$-\frac{1}{3\mathbf{K}}(1-\rho)(\delta\hat{p}\mathbf{I}:\mathbf{C}:d\varepsilon + \delta\varepsilon:\mathbf{C}^T:Id\hat{p}) \qquad (2.19)$$

$$\left.-\frac{1}{\mathbf{K}}(1-\rho)\delta\hat{p}d\hat{p} + \tilde{\boldsymbol{\sigma}}:d\delta\varepsilon + \overline{\boldsymbol{\sigma}}:(\delta\varepsilon d\mathbf{W} - d\mathbf{W}\delta\varepsilon)\right\}dV$$

The initial stress term can be approximated by

$$\tilde{\boldsymbol{\sigma}}:(d\delta\varepsilon + \delta\varepsilon d\mathbf{W} - d\mathbf{W}\delta\varepsilon)dV$$

which can be written:

$$\tilde{\boldsymbol{\sigma}}:\left[\left(\frac{\partial\delta\mathbf{u}}{\partial\mathbf{x}}\right)^T\cdot\frac{\partial du}{\partial x} - 2\delta\varepsilon.d\varepsilon\right] \qquad (2.20)$$

so that the final expression for the rate of virtual work becomes

$$d\delta\overline{\mathbf{W}} = \int_V \left\{ \delta\varepsilon : \mathbf{C} : d\varepsilon - \frac{1}{9\mathbf{K}}(1-\rho)\delta\varepsilon : \mathbf{C^T} : \mathbf{II} : \mathbf{C} : d\varepsilon + \delta\varepsilon : \overline{\boldsymbol{\sigma}}I : d\varepsilon \right.$$

$$-\frac{1}{3\mathbf{K}}(1-\rho)(\delta\hat{p}\mathbf{I} : \mathbf{C} : d\varepsilon + \delta\varepsilon : \mathbf{C}^T : \mathbf{I}d\hat{p})$$

$$\left. -\frac{1}{\mathbf{K}}(1-\rho)\delta\hat{p}d\hat{p} + \tilde{\boldsymbol{\sigma}} : \left[\left(\frac{\partial\delta\mathbf{u}}{\partial\mathbf{x}}\right)^T . \frac{\partial du}{\partial x} - 2\delta\varepsilon.d\varepsilon \right] \right\} dV \qquad (2.21)$$

The asymmetric term $\delta\varepsilon : \overline{\sigma}I : d\varepsilon$ is significant only if large volume changes occur. Hence, the term is ignored except for material models with volumetric plasticity, such as the Drucker-Prager model and the Cam-clay model. For these models the constitutive matrix $\mathbf{C}$ is usually asymmetric anyway so that the addition of this non-symmetric term does not affect the cost of analysis. It was assumed in the expression for $d\delta\lambda$ that the moduli change only slowly with change abruptly. This may lead to slow convergence or even convergence failures. Failures usually occur only in higher-order elements, since in lower-order elements $\Delta p - \Delta\hat{p}$ approaches zero at every point and the error in $d\delta\lambda$ have no impact (ABAQUS, 2005).

2.6 Contact Modeling

Initially a baseline elastic modulus was assigned to the entire lens stroma of 1.68×10^{-4} N/mm^2; i.e., the cortex and nucleus were treated as one unit. The modulus for the lens stroma was varied from 0.5×10^{-4} N/mm^2 to 0.3 N/mm^2.

Then lens cortex and nucleus were modeled with baseline moduli of 1.68×10^{-4} N/mm^2 and 1.92 N/mm^2, respectively. These elastic moduli were varied from 0.5×10^{-4} N/mm^2 to 8×10^{-4} N/mm^2,

Since it is possible that there is a relative slide between the regions of lens capsule/cortex and cortex/nucleus is possible, nonlinear contact elements were used to model the contact between the mentioned regions.

Figures 2.12 and 2.13 show the location of the contact elements for the different states of analysis.
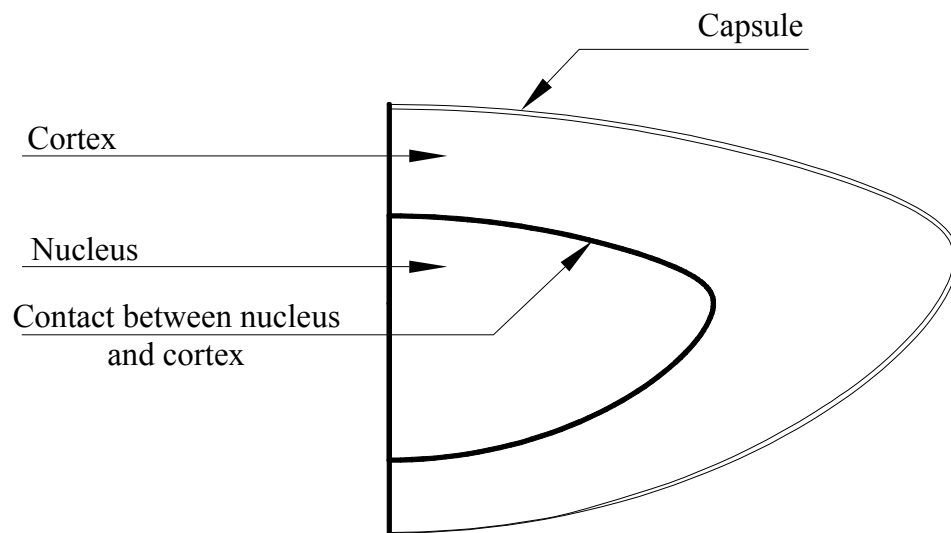
Figure 2.12 The crystalline lens model with contacts placed between the nucleus and cortex
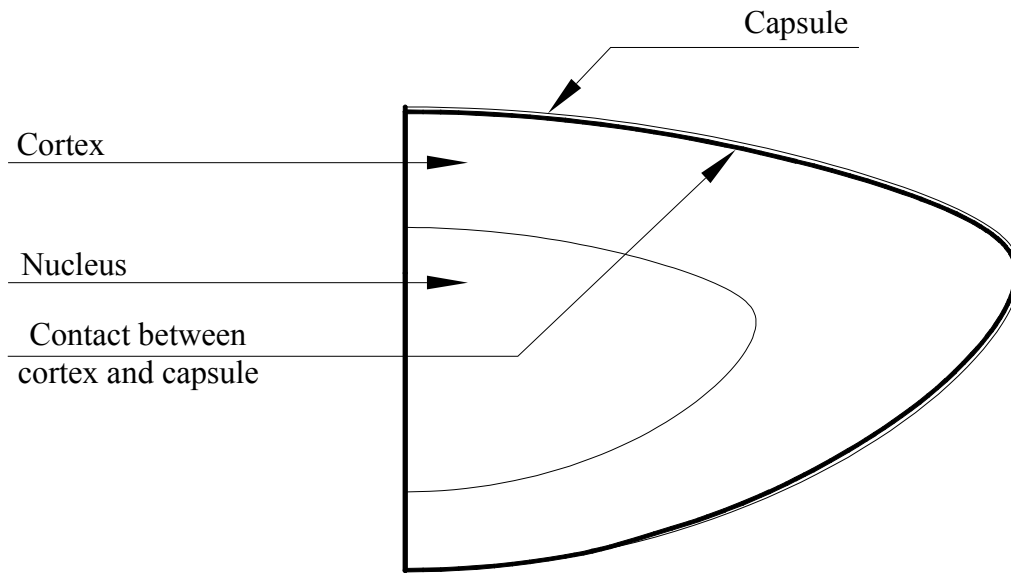
Figure 2.13 The crystalline lens model with contact placed between the cortex and capsule

2.7 Loading History

The ciliary muscle surrounds the perimeter of the equator of the lens. The ciliary muscle is located within the ciliary body. The force generated by ciliary muscle contraction is transmitted via collagen fibers within the ciliary body to the surface of the ciliary body where the zonules are attached. The tension developed within the zonules, as a result of ciliary muscle contraction, is transmitted to their attachments to the lens capsule.

There are three different zonules. Both the anterior and posterior zonules originate in the posterior part of the ciliary body (pars plana) and run forward to the anterior part of the ciliary body. They separate at the anterior part of the ciliary body to insert into the lens capsule. The anterior zonules are attached to the lens capsule anterior

to the lens equator and the posterior zonules are attached to the lens capsule posterior to the lens equator. The equatorial zonules originate in the anterior part of the ciliary body and are attached to the lens capsule at the lens equator. As the lens grows from its equator, the location of the attachments of the anterior and posterior zonules to the capsule is shifted away from the lens equator. The capsular attachment of the anterior zonules is shifted more anterior and the posterior capsular attachment is shifted more posterior with age.

The effect of traction applied by only the equatorial zonules, simultaneously by the anterior and posterior zonules, and by all three sets of zonules was assessed.

2.7.1 Zonular Traction Applied By Only The Equatorial Zonules

To model the application of zonular traction by only the equatorial zonules a displacement was applied to the lens equator with a single line-load. The other end of the line-load represents the movement of the ciliary body. The x and y coordinates of the baseline position of the ciliary body was defined in the FEM software. From this baseline position, the ciliary body was incrementally displaced outwardly, in the positive x direction, for a total of 1.125 mm. The FEM program defined the size of each incremental step.
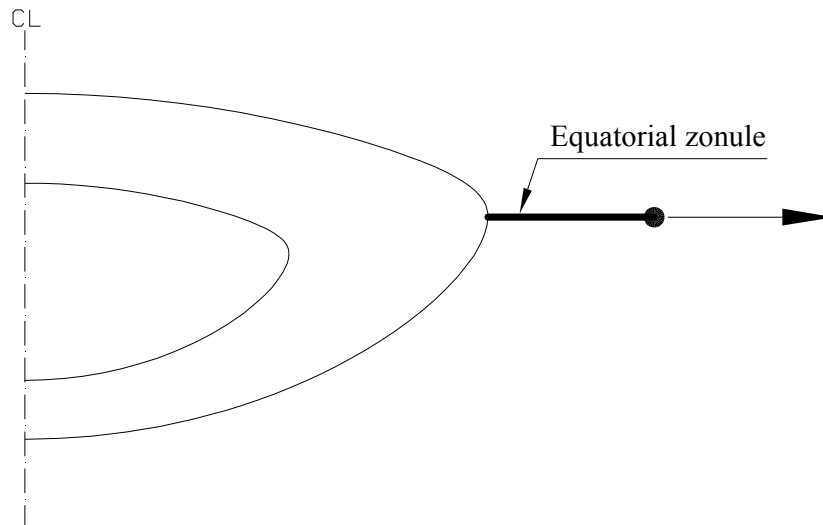
Figure 2.14 The crystalline lens is pulled by equatorial zonule

The equatorial zonule was assigned an elastic modulus of 1.5 MPa (van Alpern and Graebel, 1991), which was varied from 0.25 MPa to 3 MPa.

2.7.2 Zonular Traction Applied Simultaneously By The Anterior And Posterior Zonules
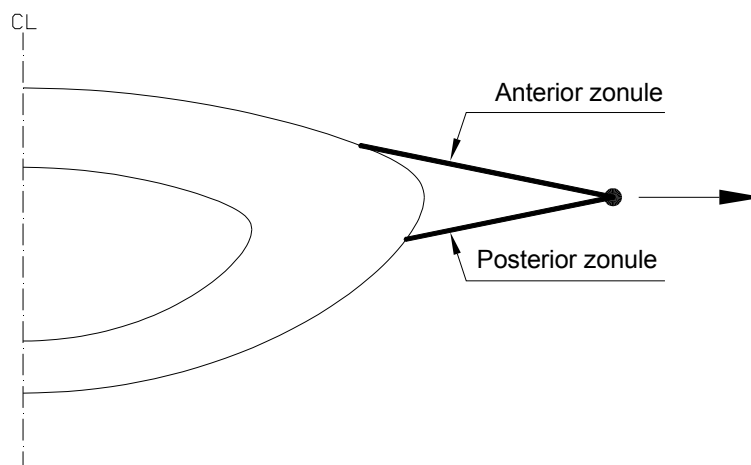
Figure 2.15 The crystalline lens is pulled by anterior and posterior zonules

45

The anterior and posterior zonules were each modeled as line-loads that meet at the equatorial plane of the lens as shown in Figure 2.14). The baseline location of the capsular attachment of the anterior zonule was 1.5 mm anterior to the lens equator and the capsular attachment was 0.75 mm posterior to the lens equator. The location of these capsular attachments was varied from 1.5 mm to 0.5 mm and 0.75 mm to 0.25 mm, respectively. The baseline elastic modulus for these zonules was 1.5 MPa

2.7.3 Zonular Traction Applied Simultaneously By All Three Sets Of Zonules

The three line-loads as listed above were combined to model the effect of simultaneous traction by all three sets of zonules. The baseline location of the attachment of the anterior and posterior zonules to the lens capsule was 1.5 mm anterior and 0.75 mm posterior to the lens equator. The location of these attachments was varied from 1.5 mm to 0.5 mm, and 0.75mm to 0.25 mm, respectively. The baseline elastic modulus for these zonules was 1.5MPa.

To duplicate of Burd et al. (2002) models, the same zonular stiffness as they used was incorporated in the model. Specifically, the anterior, equatorial and posterior zonules were assigned stiffness of 0.066N/mm 0.011N/mm, and 0.33N/mm, respectively.

46
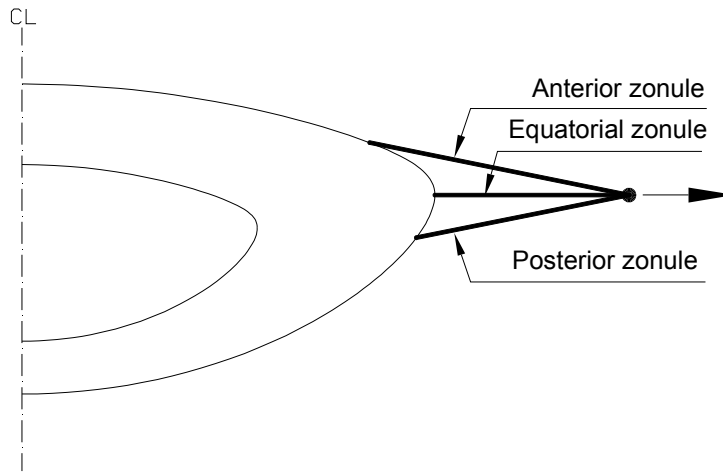
Figure 2.16 The crystalline lens is pulled by equatorial, anterior and posterior zonules

2.7.4 Boundary Conditions

Boundary conditions are only applied at the central line where the nodes are not permitted to move. The nodes and surfaces at any other place on the profile can freely move and rotate in two-dimensions.
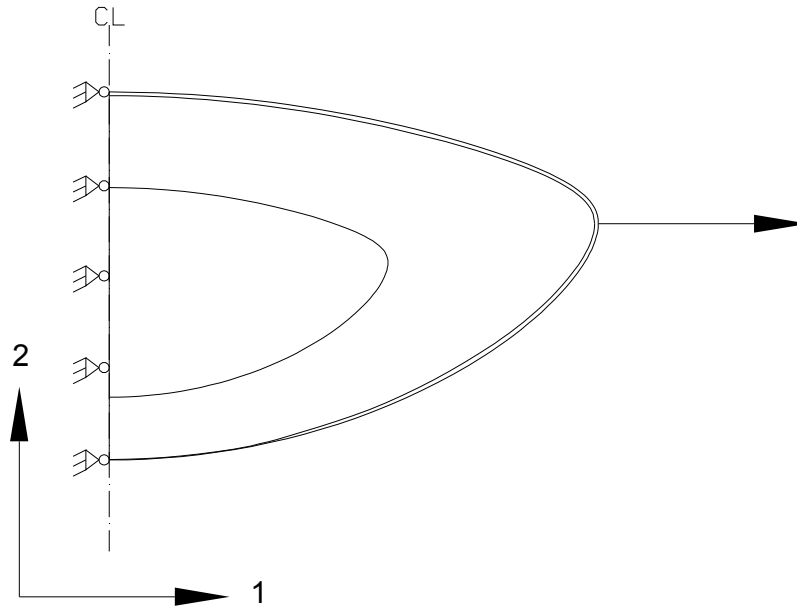
Figure 2.17 Crystalline model showing the boundary conditions.

2.8 Validation of the FEM Results

The change in central optical power of the 40y/o (19 diopters) lens associated with zonular traction applied by only the equatorial zonules was compared to an exact analytical solution given by Chien et al. (2005). The converged results are almost identical to those obtained with the exact solution are shown in Fig 3.1). When 2113 stromal quadrilateral hybrid elements and 118 capsular quadrilateral elements are used the results are almost identical to those obtained when 4870 stromal quadrilateral hybrid elements and 201 capsular quadrilateral elements are used (i.e. there is P, H, P-H convergence are reached). Therefore, the mesh with 2113 stromal and 118 capsular quadrilateral elements is identified as the converged mesh. This 40y/o (19 diopters) lens was used as the baseline reference lens from which all parameters were assessed. In addition, this lens was compared to the other lens profiles.

CHAPTER 3

PARAMETRIC STUDY

3.1 Introduction

In this chapter, a parametric study is conducted to study the effects of geometric and force related variables on the central optical power of the human crystalline lens. Also, the effect of relative sliding between the capsule and cortex is studied by placing contact elements in the interface between the two. The force related variables were the stiffness of the capsule, cortex, nucleus and zonules.

The geometric related variables were the capsule and central thickness of the lens. Six lens profiles including Lizak, Krueger A, Krueger B, Strenk A, Strenk B and Trial lens were used in the parametric study. This chapter also presents the effect of modeling the lens capsule with triangular versus quadrilateral elements on lens behavior. The effect of the number of zonules and the location of their attachment to the lens capsule were also studied. The crystalline lens equator was pulled by equatorial zonules; then simultaneously by anterior and posterior zonules; and finally by anterior, posterior and equatorial zonules. The results of the response to zonular traction applied by the equatorial zonules were compared to the exact solution reported by Chien et al., 2005.

For the parametric study the lens is modeled using quadrilateral hybrid elements for the nucleus and cortex and linear-bilinear quadrilateral elements for capsule. The

converged mesh as discussed in Chapter 2 contained approximately 2100 elements in the stroma and 118 elements in the capsule. This converged mesh was used through out the parametric study. The change in central optical power in response to zonular traction (ciliary body displacement) was the outcome variable for the parametric study.

Furthermore, this study is determined the critical geometrical and material properties of lenticular accommodation. A parametric study is performed using the change in central optical power in response to zonular traction (ciliary body displacement).

3.2 Definition of Parameters

Parameters defining the geometric variables of the lens are based on the following Equation 3.1 given by Chien et al., 2003 for the profile of the lens:

$$y(x) = \left[b + c \left(\sin^{-1}\left(\frac{x}{a}\right) \right)^2 + d \left(\sin^{-1}\left(\frac{x}{a}\right) \right)^4 \right] \cdot \cos\left(\sin^{-1}\left(\frac{x}{a}\right) \right) \qquad (3.1)$$

Table 3.1 and Figure 3.1 present the parameters based in Equation 3.1 for the six profiles used in the parametric study. Table 3.2 shows the range of the force related variables used. Each parameter was assigned a baseline value that was within the range of normally observed measurements. These measurements were obtained from the most recent literature and include *in vivo* and *in vitro* measurements of only the human crystalline lens. Measurements obtained *in vivo* and from fresh postmortem lenses were preferred.
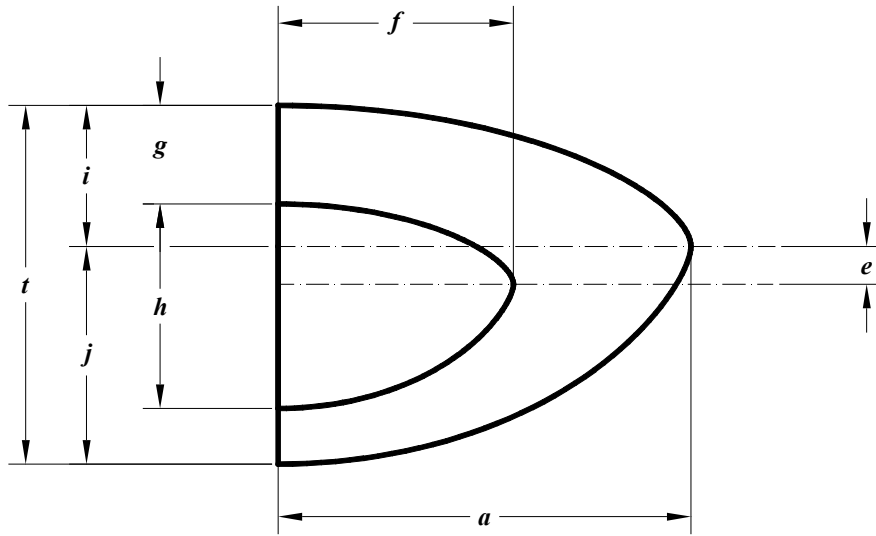
Figure 3.1 The crystalline lens geometrical properties

Table 3.1 The normal and critical values for each parameter

Parameter	Normal	Critical
Stromal Stiffness	1.7×10^{-4} N/mm^2	$> 4.0 \times 10^{-4}$ N/mm^2
Cortical Stiffness	1.7×10^{-4} N/mm^2	$> 4.0 \times 10^{-4}$ N/mm^2
Nucleus Stiffness	2.2×10^{-4} N/mm^2	$> 8.0 \times 10^{-4}$ N/mm^2
Capsular Stiffness	1.5 N/mm^2	< 0.25 N/mm^2
Zonular Stiffness	1.5 N/mm^2	< 0.1N/mm^2

Table 3.2 Baseline geometrical properties

Profile		40y/o (Krueger A) (20.7 diop.)	40y/o (KruegerB) (23.5 diop)	60y/o (Lizak) (19.3 diop.)	~20y/o (StrenkA) (21.2 diop.)	~20y/o (StrenkB) (29.0 diop.)	(Trial lens) (18.0 diop.)
Coefficients for Anterior Profile (Equation 3.1)	a	4.485	4.2815	4.5	4.5	4.3	4.3
	b	1.2089032	1.463629	1.55467	1.43966686	1.75102	1.9
	c	-0.266892	-0.166822	-0.329	-0.0962011	-0.130361	0.1795833
	d	0.1166546	-0.021135	0.08141	0.11256773	0.117481	-0.3848683
Coefficients for Posterior Profile (Equation 3.1)	a	4.485	4.2815	4.5	4.5	4.3	4.3
	b	2.1669011	2.260218	2.27038	2.37778017	2.628273	2.0
	c	-0.368996	-0.259828	-0.6326	-0.5892980	-0.964052	-0.1929032
	d	0.0006791	-0.114285	0.0869	0.15832193	0.311269	-0.2503307
Dimensions for the Lens Outline (see Figure 3.1) (mm)	a	4.4850	4.2815	4.5	4.5	4.3	4.3
	e	0.3570	0.3938	0.4045	0.4037	0.4631	0.4045
	f	2.5565	2.4405	2.3850	2.7900	2.6660	2.8504
	g	0.8768	1.0232	1.1352	0.9508	1.1285	0.9714
	h	1.9242	2.1226	2.0273	2.3668	2.7152	2.4180
	i	1.2089	1.4636	1.5547	1.4397	1.7510	1.90
	j	2.1669	2.2602	2.2704	2.3778	2.6283	2.0
	t	3.3758	3.7238	3.8250	3.8174	4.3793	3.90

All the baseline parameters were chosen for the 40 year old Krueger A lens.

The anterior central capsular thickness increases through out life. The central posterior capsule does not change thickness. The range of anterior central capsular thickness is 5 to 35 microns. Based on the measured in vitro age-related changes in thickness, the assigned baseline central anterior lens capsular thickness is 23.92 microns (Krag and Andreassen, 2003). For the parametric study the anterior central capsular thickness was varied from 5 to 50 microns.

The posterior capsule does not change thickness. The assigned baseline value is 5 microns (Krag and Andreassen, 2003). For the parametric study the thickness of the central posterior capsule was held constant at 5 microns.

The elastic modulus of the capsule changes from 0.75 to 1.5 MPa from birth to 35 years of age and then remains constant (Krag and Andreassen, 2003). A baseline elastic modulus of 1.5 MPa was assigned. For the parametric study the elastic modulus of the anterior capsular modulus was varied from 0.25 MPa to 3 MPa.

The elastic modulus remains constant through life at 0.75 MPa. A baseline elastic modulus of 1.5MPa was assigned. For the parametric study the elastic modulus of the posterior capsule was held constant at 0.75 MPa.

For the lens stroma the cortex and nucleus were treated as one unit with the same elastic modulus. The assigned elastic modulus was based on *in vivo* measurements of the speed of ultrasound through the center of the lens, $c = 1649/m/sec$ which was found to be invariant between the ages of 15 and 45 years of age (Beers and van der Heijde, 1994). Using the formula for bulk modulus, $K = pc^2$ where $\rho = 1032\ kg/m^3$, is lens density (Duck, 1990) the bulk modulus of the lens is 2.8GPa. From measurements of pieces of thawed lenses following freezing in liquid nitrogen the shear modulus is ~ 50 Pa.

From the formulas relating bulk modulus and shear modulus, G to the elastic modulus, E:

$$E = 3K(1 - 2v) \tag{3.2}$$

$$E = 2G(1 + v) \tag{3.3}$$

to the elastic modulus, the Poisson's ratio $v = 0.49999999$. Therefore, from Equation 3.2 the elastic modulus for the lens stroma is 1.68×10^{-4} MPa. A baseline elastic modulus of 1.68×10^{-4} MPa was assigned. For the parametric study the range of the elastic modulus for the lens stroma was varied from 0.5×10^{-4} MPa to 4×10^{-4} MPa.

The bulk modulus of the lens cortex is $K = 2.8$ GPa as measured non-invasively using Brillouin light scattering in fresh human lenses *in vitro*. Using Equation 3.2 and the above Poisson's ratio the cortex was assigned a baseline value of 1.68×10^{-4} MPa. For the parametric study the elastic modulus of the lens cortex was varied from 0.5×10^{-4} MPa to 4×10^{-4} MPa.

The bulk modulus of the lens nucleus is $K = 3.7$ GPa as measured non-invasively using Brillouin light scattering in fresh human lenses in vitro. Using Equation 3.2 and the above Poisson's ratio the nucleus has an elastic modulus of 2.22×10^{-4} MPa. The nucleus was arbitrarily assigned a baseline value of 1.92×10^{-4} MPa. For the parametric study the elastic modulus of the nucleus was varied from 0.5×10^{-4} MPa to 8×10^{-4} MPa.

The zonules were assigned a baseline elastic modulus of 1.5 MPa (van Alpern and Greabel, 1991). For the parametric study the elastic modulus of the zonules was varied from 0.1 MPa to 3MPa.

The attachment points of the anterior and posterior zonules to the lens capsule shift away from the lens equator as the lens grows with age from its equator. The values of baseline capsular attachment of the anterior and posterior to equatorial zonules were

54

1.5 and 1.0, respectively. The arc length from the equator of the location of the attachment of the anterior zonules to the lens capsule was varied from 0.5 to 1.5 mm. Similarly, the arc length from the equator of the location of the attachment of the posterior zonules to the lens capsule was varied from 0.25 to 0.75 mm.

3.3 Central Optical Power

The central optical power is given by:

$$Central\ Optical\ Power (diopters) = \frac{n_1 - n_a}{r_a} + \frac{n_1 - n_a}{r_p} - \frac{t \cdot (n_1 - n_a)^2}{r_a \cdot r_p \cdot n_1} \qquad (3.4)$$

Where r_a and r_p is the radius of curvatures of the central anterior and posterior lenticular surface, respectively, which are calculated by using 1.6 mm diameter aperture (Burd et al., 2002). The values of $n_1 = 1.42$ (Jones et al., 2005), $n_a = 1.336$, and t (the lens thickness at the pole) is used in calculating optical power from Equation 3.4.

3.4 Range of Force and Geometric Parameters

For the parametric study the converged mesh (Chapter 2) is used, which is shown in Figure 3.2.

The elastic modulus of nucleus was changed as follows: 5×10^{-5}; 1.68×10^{-4}; 1.92×10^{-4}; 4×10^{-4}; and 8×10^{-4} N/mm^2 while the modulus of cortex was kept at constant values of 1.68×10^{-4} N/mm^2. The elastic modulus of capsule was 1.5 N/mm^2 for anterior surface and 0.75 N/mm^2 for posterior surface. The crystalline lens was pulled by the central (equatorial) zonules, with an assigned stiffness of 1.5 N/mm.

Similar to nucleus, the following elastic moduli were used for the nucleus: 0.5×10^{-4}; 1.68×10^{-4}; 1.92×10^{-4}; 4×10^{-4}; and 8×10^{-4} N/mm^2 while the modulus of nucleus

55

was kept constant at 1.92 x10^{-4} N/mm^2. Moreover, the elastic modulus of the capsule was 1.5 N/mm^2 for the anterior surface and 0.75 N/mm^2 for the posterior surface. The crystalline lens was pulled by the equatorial zonules with an elastic modulus of 1.5 N/mm^2.
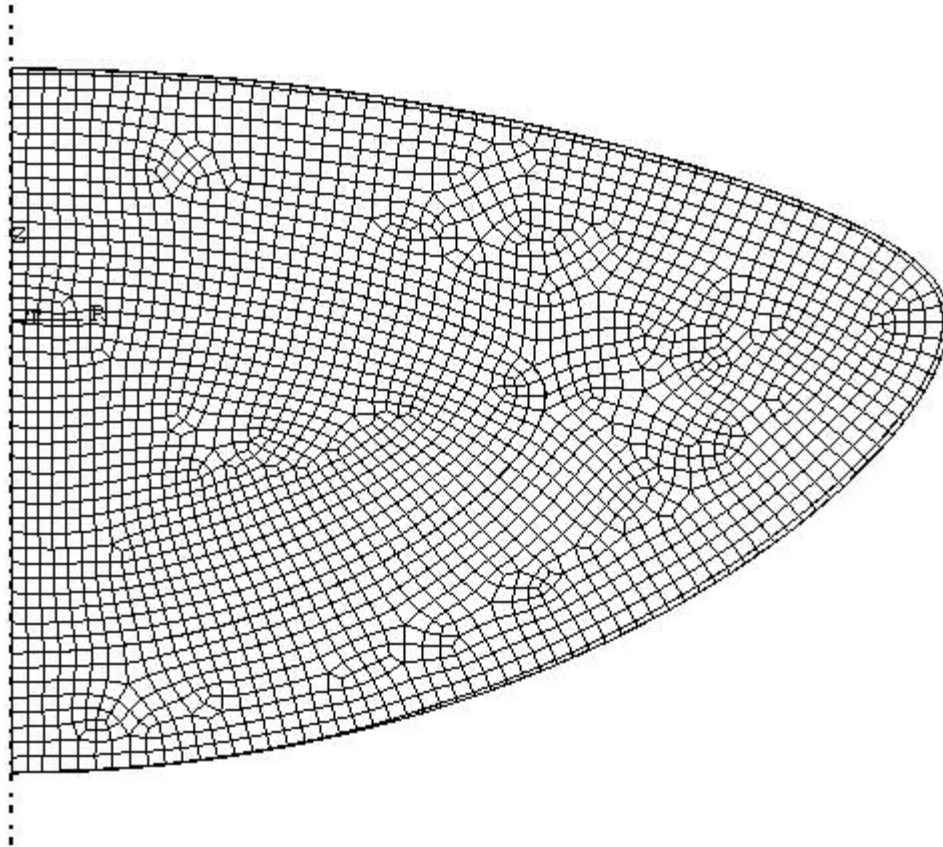
Figure 3.2 The converged mesh of 40 y/o (Krueger profile A)

Stroma is the term used to represent both the nucleus and cortex.

CL

Capsule thickness

Joined nucleus and cortex (stroma)
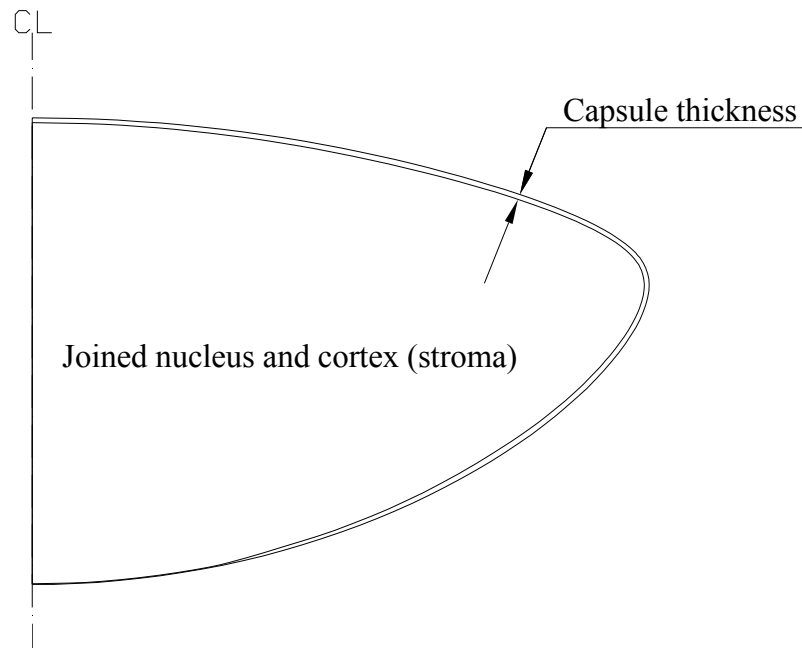
Figure 3.3 The crystalline lens model - joined nucleus and cortex (stroma)

3.5 Study Results and Discussion

3.5.1 Validation

The developed model is validated because the results of the converged FEM mesh duplicate the exact solution for the 40 y/o Krueger A lens (Figure A.1) (Chien et al., 2005).

3.5.2 Zonular Traction

Zonular traction, beginning at zero, applied by only the equatorial zonules results in an increase in central lenticular optical power (Figure A.1), and central thickness (Figure A.14) which both peak and then decrease with further traction independent of baseline accommodative state or age of the lens (Figure A.12).

57

When traction is applied simultaneously by the anterior and posterior zonules or all three sets of zonules (Figure A.13), there is also an increase in central optical power, which reaches a maximum, and then declines with increased traction. However, more force is required (Figure A.15), and the change in optical power is significantly less than occurs with only equatorial zonular traction. The increase in central optical power associated with anterior and posterior zonular traction occurs even if the location of their attachments to the lens capsule is varied (Figure A.13). In addition, traction by these zonules monotonically decreases central lenticular thickness (Figure A.14).

3.5.3 Material Properties

The reaction of central lenticular optical power to equatorial zonular traction is considerably reduced when rigidity of either: the total lens stroma, or cortex is larger than $4x10^{-4}$ N/mm^2, or nucleus is larger than $8x10^{-4}$ N/mm^2, or capsule is smaller than 0.25 N/mm^2, or zonules is less than 0.1 N/mm^2 (Figure A.3 and Figure A.4) and (Table 3.1).

3.5.4 Geometric Properties

A thicker capsule augments the enlargement in central optical power associated with equatorial zonular traction (Figure A.5). On the other hand, neither central lens thickness (Figure A.7); baseline intralenticular pressure (Figure A.9); or the placement of contact elements between the nucleus and cortex, or between the capsule and cortex have a significant effect (Figure A.10 and Figure A.11).

3.5.5 Discussion

Zonular traction starting at zero increases central lenticular optical power whether the traction is applied only by the equatorial zonules, or simultaneously by the anterior and posterior zonules or all three sets of zonules. The raise in central optical power reaches a maximum and then declines with increased traction. Equatorial zonular traction increases central optical power significantly more than traction applied by the anterior and posterior zonules or all three sets of zonules.

Initial equatorial zonular traction increases central lenticular thickness which peaks and then decreases with more traction. On the contrary, central thickness declines linearly when zonular traction is applied all together by the anterior and posterior zonules or all three sets of zonules.

Our results are consistent with other models (Schachar and Bax, 2001; Shung, 2002, Chien et al., 2005), but differ from Burd's et al. (2002). Burd et al. (2002) used a discontinuous function for the lens profile consisting of a fifth order polynomial, a straight line, and a circular end cap. An unrealistic lens was used Burd et al. (2002) with cortical/nuclear stiffness ratio of 6.2 to model a 29y/oacc lens; i.e., the cortex of this lens was 6 times harder then its nucleus. Brillouin light scattering (Subbaram et al., 2002) and dynamometric measurements of *in vitro* fresh human lenses (Nordmann et al., 1974) and routine clinical observation during *in vivo* cataract extraction by phacoemulsification demonstrate that the hardness of the nucleus of lenses older than 25 years is either the same or greater than its cortex (Kelman, 1976).

We duplicate Burd's et al (2002) analysis of the 29y/oacc lens by employing the same unrealistic moduli, and a coarse unconverged mesh with identical type of elements (Figure A.16). Then, we demonstrate that zonular traction, beginning at zero, increases central optical power when a converged solution are used with appropriate elastic moduli for the cortex and nucleus (Figure A.16).

Increasing capsular stiffness increases the change in central optical power induced by zonular traction. Therefore, it is unlikely that the age-related increase in capsular stiffness is the etiology of presbyopia. This is consistent with the predictions of Krag and Andreassen (2003a) and the observation that from birth to 35 years of age the capsule becomes stiffer; however, from 35 to 60 years old the stiffness of the capsule does not change (Krag and Andreassen, 2003a, 200b). Even though there is no change in lens capsule stiffness in the older group the accommodative amplitude declines equally, by approximately 7 diopters, in both age groups (Duane, 1917).

Throughout life the thickness of the capsule increases (Krag and Andreassen, 2003a). A thicker capsule increases the change in central optical power of the lens to zonular traction. Therefore, neither an increase in capsular thickness nor stiffness appears to be the etiology of presbyopia.

Central lens thickness does not influence the change in central optical power associated with equatorial traction. This is consistent with the study that central lenticular thickness decreases from birth until the second decade and then increases with age (Schachar, 2005b), while accommodative amplitude is linearly declining with age (Duane, 1917).

60

Between the ages of 15 and 44 years the bulk modulus of the normal lens is constant as demonstrated by *in vivo* measurements of the speed of ultrasound (Beers and van der Heijde, 1994) and diametric measurements of *in vitro* fresh human lenses (Nordmann et al., 1974). In this age group the bulk modulus, *K = 2.8* GPa,

$$K = \rho \cdot c^2 \tag{3.5}$$

where *c = 1649 m/sec*, the mean velocity of sound in the lens for this age group (Beers and van der Heijde, 1994), and $\rho = 1032$ kg/m3, is lens density (Duck, 1990). Consistent with these calculations the bulk modulus of the cortex and nucleus of *in vitro* fresh human lenses between the ages of 30 and 63 years is 2.8 and 3.7 GPa, respectively, as measured by Brillouin light scattering (Subbaram et al., 2002). Therefore, the stiffness of the normal lens cortex and nucleus of lenses under 60 year of age is smaller than 1.7×10^{-4} and 2.2×10^{-4} N/mm^2, respectively. Stiffness measurements of the cortex and nucleus of thawed lenses after being frozen in liquid nitrogen (Pau and Kranz, 1991; Heys et al., 2004; Weeber et al., 2005) come out to be significantly higher than when fresh lenses are calculated (Nordmann et al., 1974, Subarram et al., 2002). However, even these measurements do not show a significant change in lens stiffness in lenses less than 40 y/o (Heys et al., 2004; Weeber et al., 2005; Schachar, 2005c).

We show that hardness of the entire lens stroma, or cortex, would have to be larger than 4×10^{-4} N/mm^2, and the nucleus larger than 8×10^{-4} N/mm^2 to significantly reduce the change in optical power induced by zonular traction. Therefore, it is unlikely that the normal physiological change in hardness of the cortex, nucleus or entire lens

stroma is the etiology of the 10-diopters decline in accommodative amplitude that occurs from birth to 40 years of age (Duane, 1917).

Zonular stiffness has been shown to be approximately 1.5 N/mm^2 (van Alphen and Graebel, 1991). We find that zonular stiffness would have to decrease by 15 times, to reduce the central optical power response to equatorial zonular traction.

Baseline lenticular pressure, between 0.1 and 5 mm Hg, does not appear to significantly affect the lenticular change in central optical power associated with equatorial traction. This is consistent with the smaller than 1 mm Hg applanation intralenticular pressure of freshly preserved postmortem human lenses (Schachar, 2005d).

The FEM prediction that zonular traction beginning from zero induces central anterior surface steepening is consistent with the anterior surface changes observed, when zonular traction is applied *in vitro* to human lenses (Stadfeldt, 1896; Pierscionek, 1993; Schachar, 2004), and to pharmacologically induced *in vivo* accommodation in primates (Schachar et al., 1995; Schachar and Kamangar, 2005) and in humans (Schachar et al., 1996).

Chien et al. (2005) used membrane theory in their exact solution and did not include bending because of the distance of the applied equatorial force from the center of the lens surfaces. In the present FEM analysis we used quadrilateral elements that incorporate bending (Dvorkin and Kathe, 1983). We duplicate Chien's et al (2005) results. Therefore, it comes out that their statement was acceptable.

Contact elements located between the cortex and nucleus or capsule and cortex did not notably change the response. This is consistent with the facility that lens fibers are hydro-dissected from the capsular epithelium (Nordmann et al., 1974; Rakic et al., 1997) and the lens nucleus (Ayaki and Ishii, 1993). The shear modulus of the young lens (Weeber et al., 2005; Heys et al., 2004; Hogan et al., 1971) is small. Consequently, the effect of inter-lens fiber attachments and lens sutures on the lenticular reaction to zonular traction is probably negligible; conversely, it may be considered in future analysis.

CHAPTER 4

SUMMARY AND CONCLUSION

4.1 Summary

In this study, a nonlinear finite element model (FEM) of human accommodation lens was developed using axisymmetric concept. The lens profile for FEM analysis was built by employing a continuous function, which was introduced by Chien et al. (2003). Because the crystalline lens is axisymmetric, only one half of the lens was used for modeling. After several trials an appropriate converged mesh was carefully selected for the model to represent as the best mesh for the parametric study. The elements used were quadrilateral four node hybrid for the stroma and regular quadrilateral four node for the capsule. The mesh was created by employing advancing-front-technique in ABAQUS (ABAQUS. 2005). An incremental displacement-based loading history was applied to the lens to obtain the central optical power versus ciliary body displacement; central thickness versus ciliary displacement; and zonule force versus central optical power.

To study the effect of relative movement, due to zonule traction, between the capsule and the cortex, and cortex and nucleus, contact elements was introduced in the interface between the two regions. The developed model was analyzed using incremental geometric nonlinear finite element solution algorithm. The converged

solution was obtained by integrating norm 2, II-II, and energy-based convergence criteria.

A parametric study was conducted to study the effects of force and geometry related variables on the lens's optical power. This was done by changing each variable from its low to high values while keeping other variables at their intermediate values.

The geometric related variables were assessed by using six different lens profiles: Lizak; Krueger A; Krueger B; Strenk A; Strenk B; and Trial lens. In these profiles, central thickness, capsular thickness and the location of the attachment of the zonules to the lens capsule were varied within their physiological range.

The force related variables that were varied were stiffness of the capsule; cortex; nucleus and zonules. In addition, the displacement loading was applied to the lens in three independent ways using either: the equatorial zonule; the anterior and posterior zonules; or the equatorial, anterior and posterior zonules.

4.2 Conclusions

As traction was applied simultaneously by the anterior and posterior zonules or all three sets of zonules, there was an increase in central optical power. However, more force was required, and the change in optical power was significantly less than occurred with only equatorial zonular traction. The increase in central optical power associated with anterior and posterior zonular traction occurs even if the location of their attachments to the lens capsule is varied. In addition, whenever the anterior and posterior zonules are involved in apply traction the central lenticular thickness decreases.

The reaction of central lenticular optical power to equatorial zonular traction is considerably reduced when rigidity of either: the total lens stroma, or cortex larger than 4×10^{-4} N/mm^2, or nucleus stiffness is larger than 8×10^{-4} N/mm^2, or capsular stiffness is smaller than 0.25 N/mm^2, or zonular stiffness is less than 0.1 N/mm.

A thicker capsule augments the increase in central optical power associated with equatorial zonular traction. Alternatively, neither central lens thickness; baseline intralenticular pressure; or the placement of contact elements between the nucleus and cortex, or between the capsule and cortex have a significant effect on the change in central optical power.

Equatorial zonular traction increases central optical power significantly more than traction applied by the anterior and posterior zonules or all three sets of zonules. Central thickness declines linearly when zonular traction is applied all together by the anterior and posterior zonules or all three sets of zonules.

Increasing capsular stiffness increases the change in central optical power induced by zonular traction. Therefore, it is unlikely that the age-related increase in capsular stiffness is the etiology of presbyopia.

This study showed that central lens thickness does not influence the change in central optical power associated with equatorial traction. This is consistent with the study that central lenticular thickness decreases from birth until the second decade and then increases with age, while accommodative amplitude is linearly declining with age.

It was shown that hardness of the entire lens stroma, or cortex, would have to be larger than 4×10^{-4} N/mm^2, and the nucleus larger than 8×10^{-4} N/mm^2 to significantly

reduce the change in optical power induced by zonular traction. Therefore, it is unlikely that the normal physiological change in hardness of the cortex, nucleus or entire lens stroma is the etiology of the 10-diopters decline in accommodative amplitude that occurs from birth to 40 years of age.

Zonular stiffness has been shown to be approximately 1.5 N/mm. We find that zonular stiffness would have to decrease by 15 times, in order to reduce the central optical power response to equatorial zonular traction.

Baseline lenticular pressure, between 0.1 and 5 mm Hg, does not appear to significantly affect the lenticular change in central optical power associated with equatorial traction.

The FEM prediction that zonular traction induces central anterior surface steepening is consistent with the anterior surface changes observed, when zonular traction is applied *in vitro* to human lenses, and to pharmacologically induced *in vivo* accommodation in primates and in humans.

Contact elements located between the cortex and nucleus did not notably change the response. When contact elements was placed between the capsule and nucleus for low contact normal stiffness, the optical power increased by approximately 4 % when Krueger profile A was used, however the optical power increased 16 % with the Trial lens profile. Thus, contact elements enhance the values for optical powers depending on the lens geometry. The small increase in effect noted with the placement of contact elements between the capsule and cortex is consistent with the facility that lens fibers are hydro-dissected from the capsular epithelium. The shear modulus of the young lens

is small. Consequently, the effect of inter-lens fiber attachments and lens sutures on the lenticular reaction to zonular traction is probably negligible; conversely, it may be considered in future analysis.

<div align="center">4.3 Recommendations</div>

The critical parameters for lenticular accommodation have been defined. However, an additional major parameter is baseline lens shape. The formula used in the present study best emulates the human lens; however, the critical parameters of the formula have not been determined. A parametric study to determine the effect of altering the coefficients of the formula while holding the central surface radii of curvatures constant would be of significant value.

It is recommended that the data generated from this study should be used to develop statistical equations that can predict outcomes without relying on the FEM. These equations could potentially help in the development of formulas for the lens profiles that are superior to the formulas used in the present study and also may give other insights into lenticular accommodation.

The present FEM model of lenticular accommodation should be extended to incorporate the actual connections of the zonules to the ciliary body. This should include the ciliary muscle, which is located inside the ciliary body. The ciliary muscle has multiple muscular subdivisions. Exactly how these subdivisions interact to induce zonular tension and how the forces are directed to each set of zonules is not exactly known. The FEM analysis should be able to determine the biomechanical possibilities

and the critical geometric and material properties of the ciliary body and ciliary muscle required for *in vivo* accommodation.

Once the mechanism of the ciliary muscle is understood then a complete FEM model of the eye should be constructed. This is very important because the ciliary muscle is attached to the trabecular meshwork, which is the major drainage site for aqueous humor. When this drainage site becomes blocked the pressure within the eye elevates. The elevated intraocular pressure (IOP) causes damage to the optic nerve, which if untreated, eventually leads to blindness. Glaucoma is one of the largest causes of irreversible blindness. The proposed FEM model could potentially lead to significant insights into the critical components that impede aqueous outflow and may suggest new and better treatment modalities and possible preventive measures.

It has been suggested that the occurrence and/or magnitude of nearsightedness, myopia, is influenced by the accommodative mechanism. Using the fully developed FEM model of the eye the forces that are exerted during accommodation can be determined. The biomechanical effects on the scleral shell, cornea, vitreous, and retina can be assessed to determine how the accommodative mechanism can potentially play a role in the development of myopia, astigmatism, glaucoma, and retinal detachment.

In summary, a fully developed FEM model of the eye that incorporates the present FEM analysis would have significant clinical value in understanding, preventing and treating multiple maladies of the eye.

This FEM model duplicated the increase in central optical power obtained with the analytical solution; it can attain the change in central optical power observed during

human *in vivo* accommodation by using the Trial lens profile. However the displacement at the anterior and posterior still not appropriate, thus there should be more study with the Trial lens for pole movement.

Additional studies are required to determine the critical parameters of the baseline lens shape, not evaluated in the present study, that are required to maximize the response to equatorial zonular traction. Once these baseline geometric parameters are determined, the relative movements of the anterior and posterior surfaces should be compared to *in vivo* measurements.

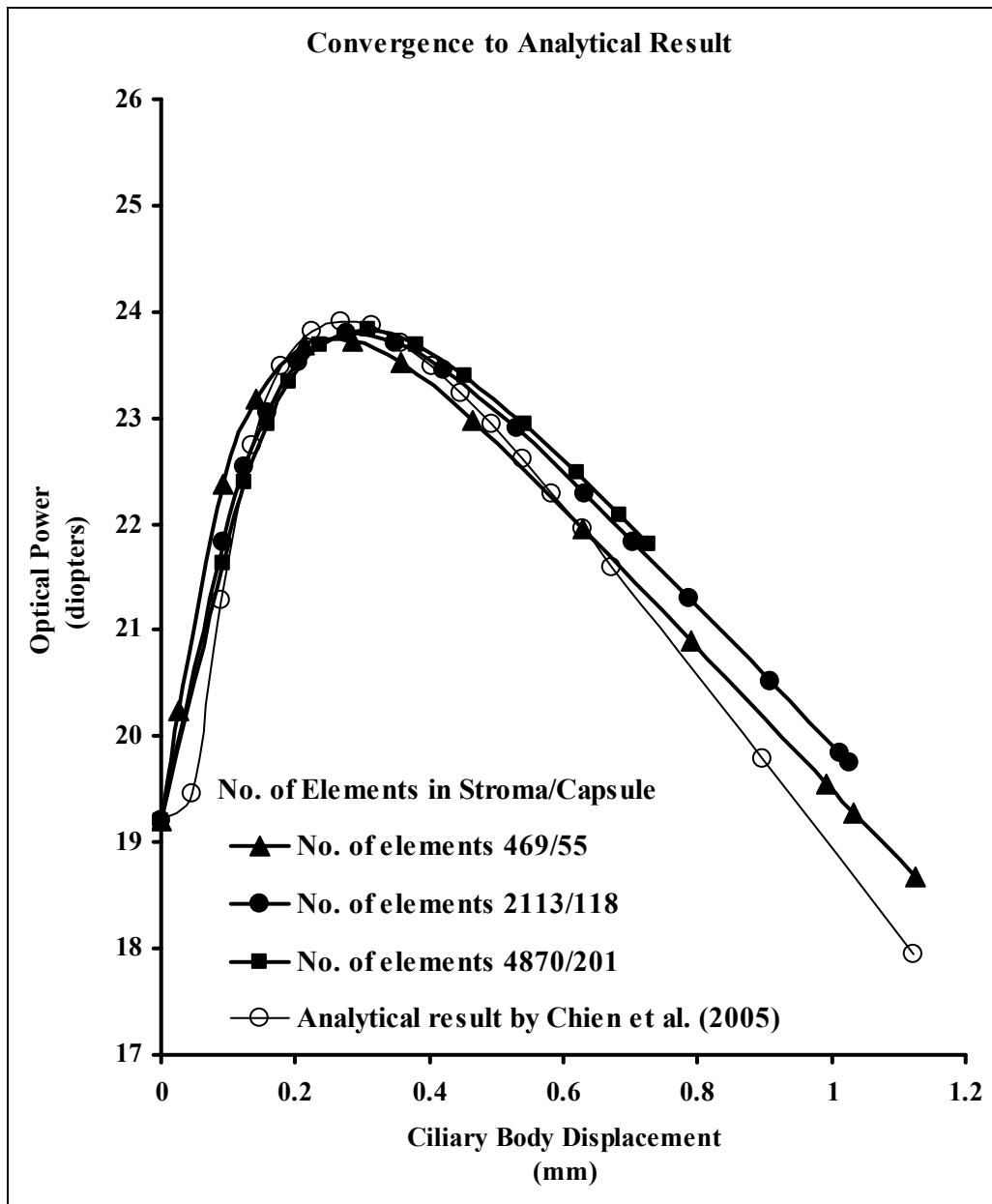APPENDIX A

PARAMETRIC STUDY RESULT PLOTS

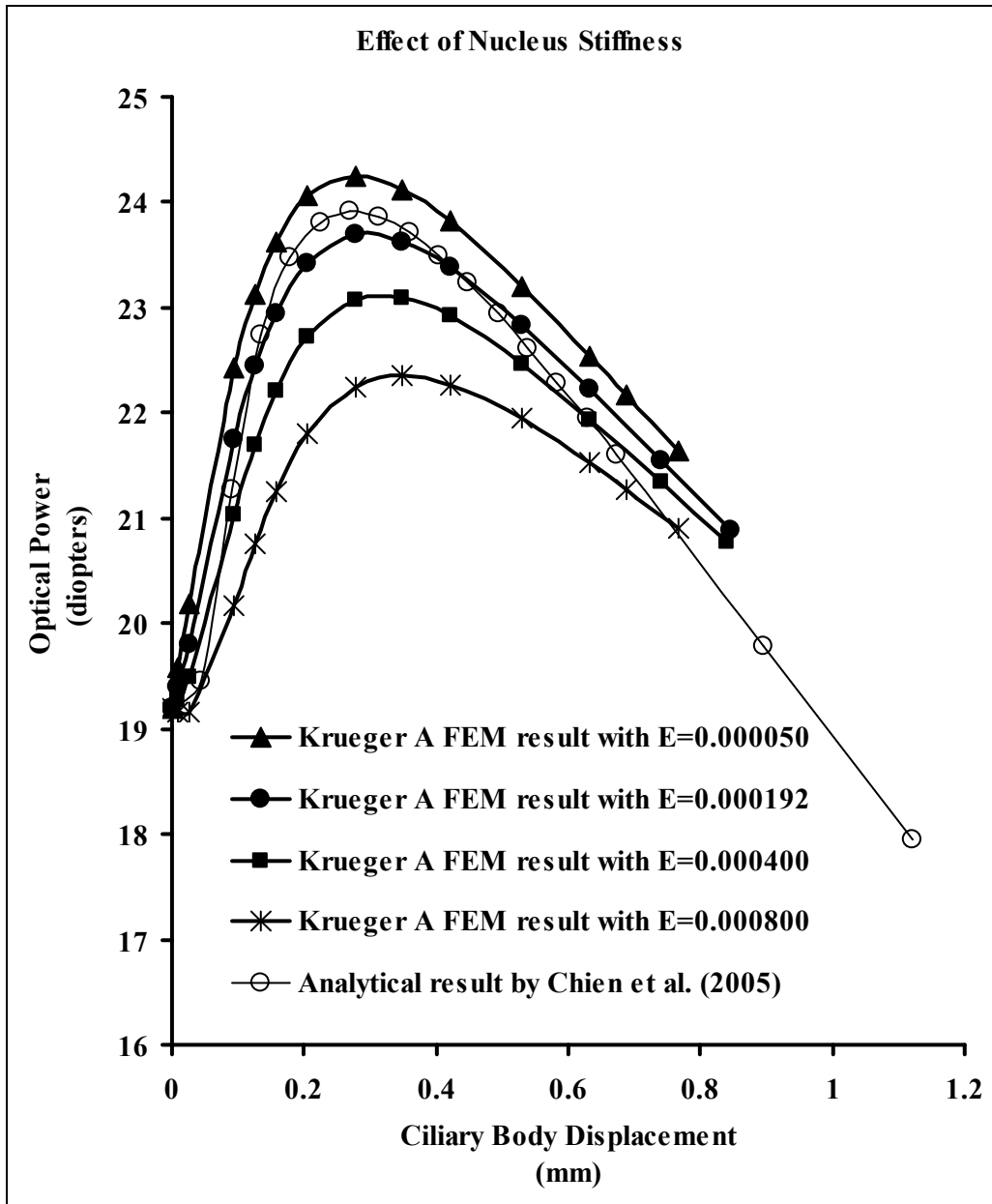Figure A.1 Optical power convergence result
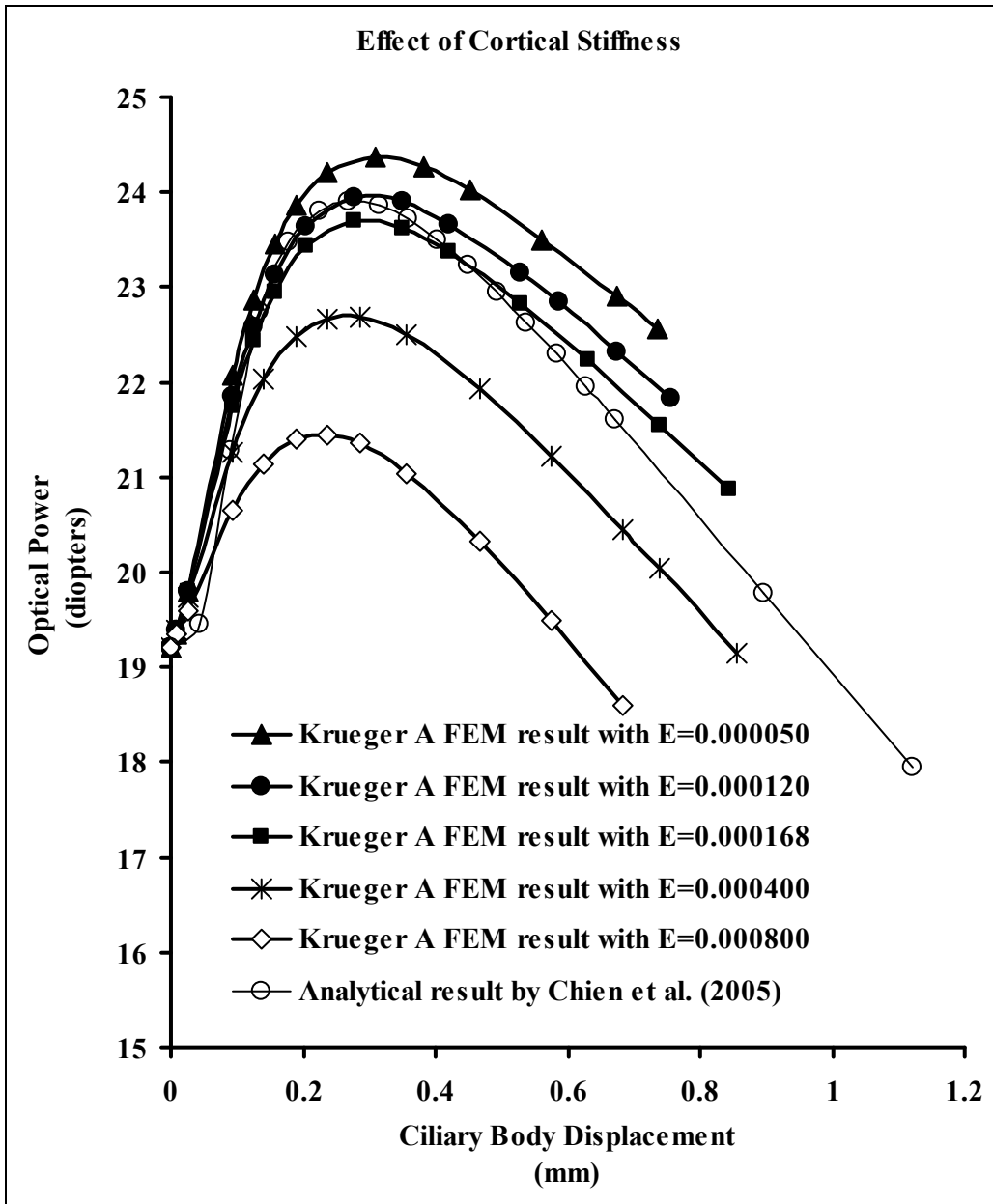
Figure A.2 Change in nucleus modulus

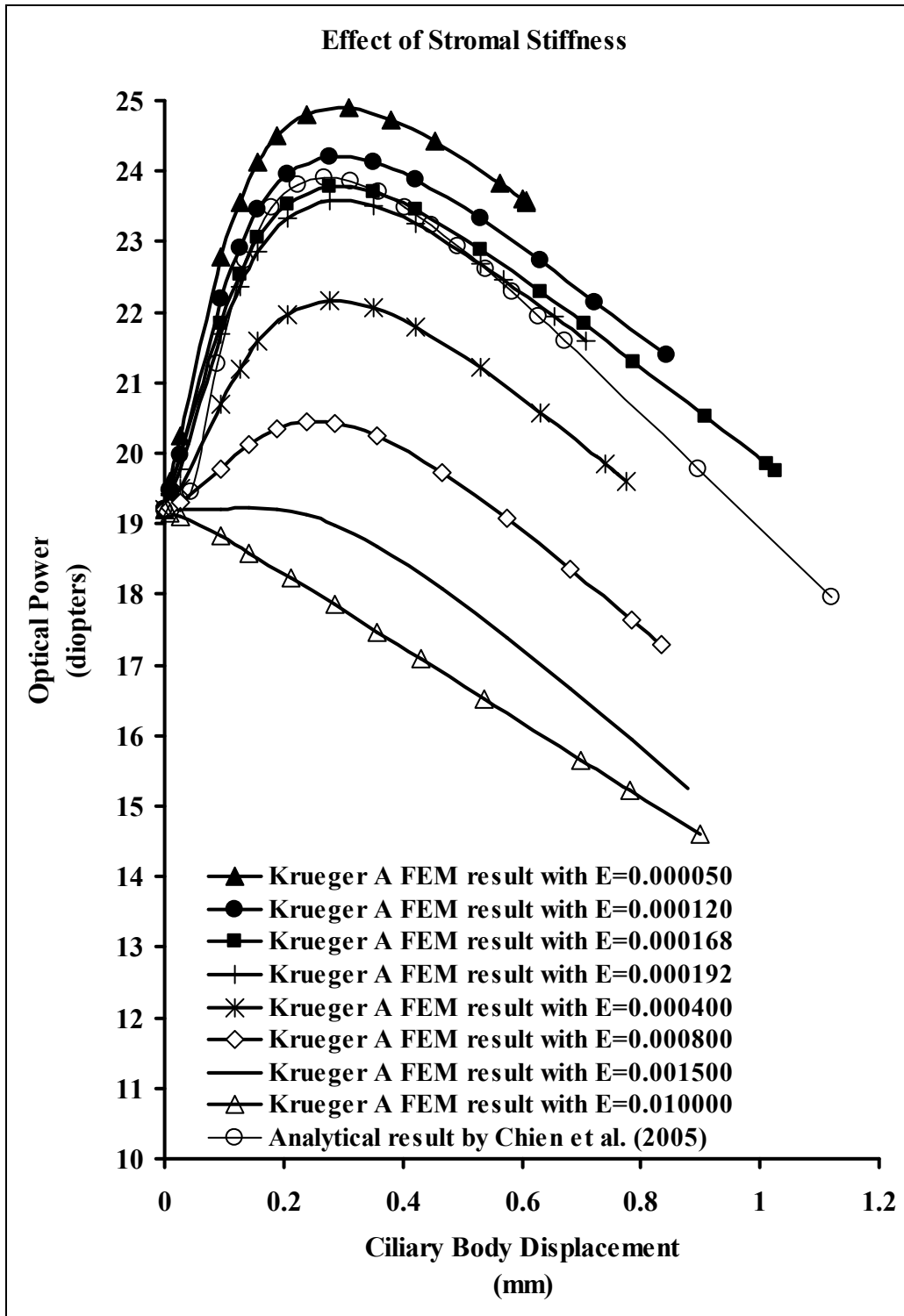Figure A.3 Change in cortex modulus

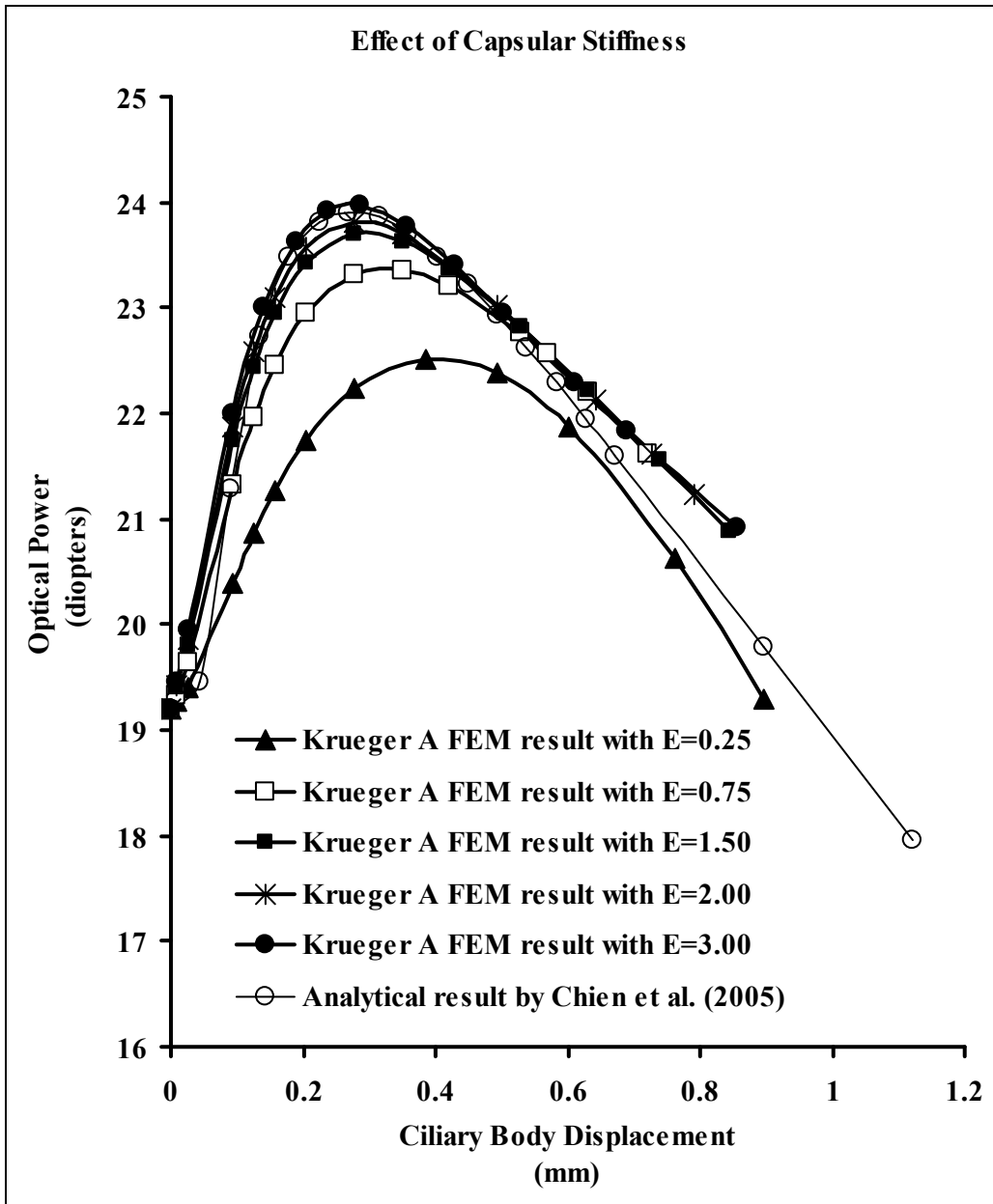Figure A.4 Change in stromal modulus
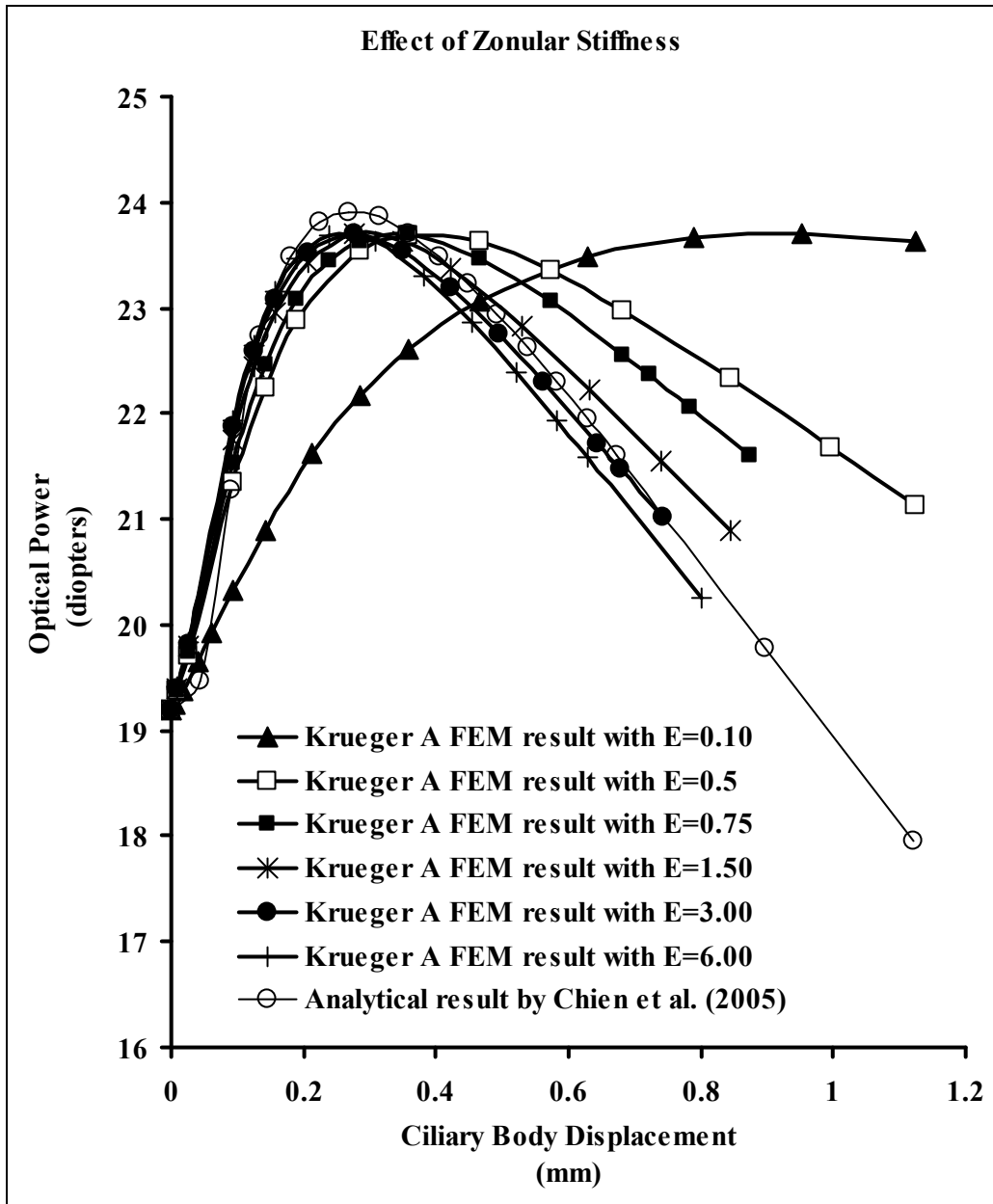
Figure A.5 Change in capsule modulus

Figure A.6 Change in zonular stiffness
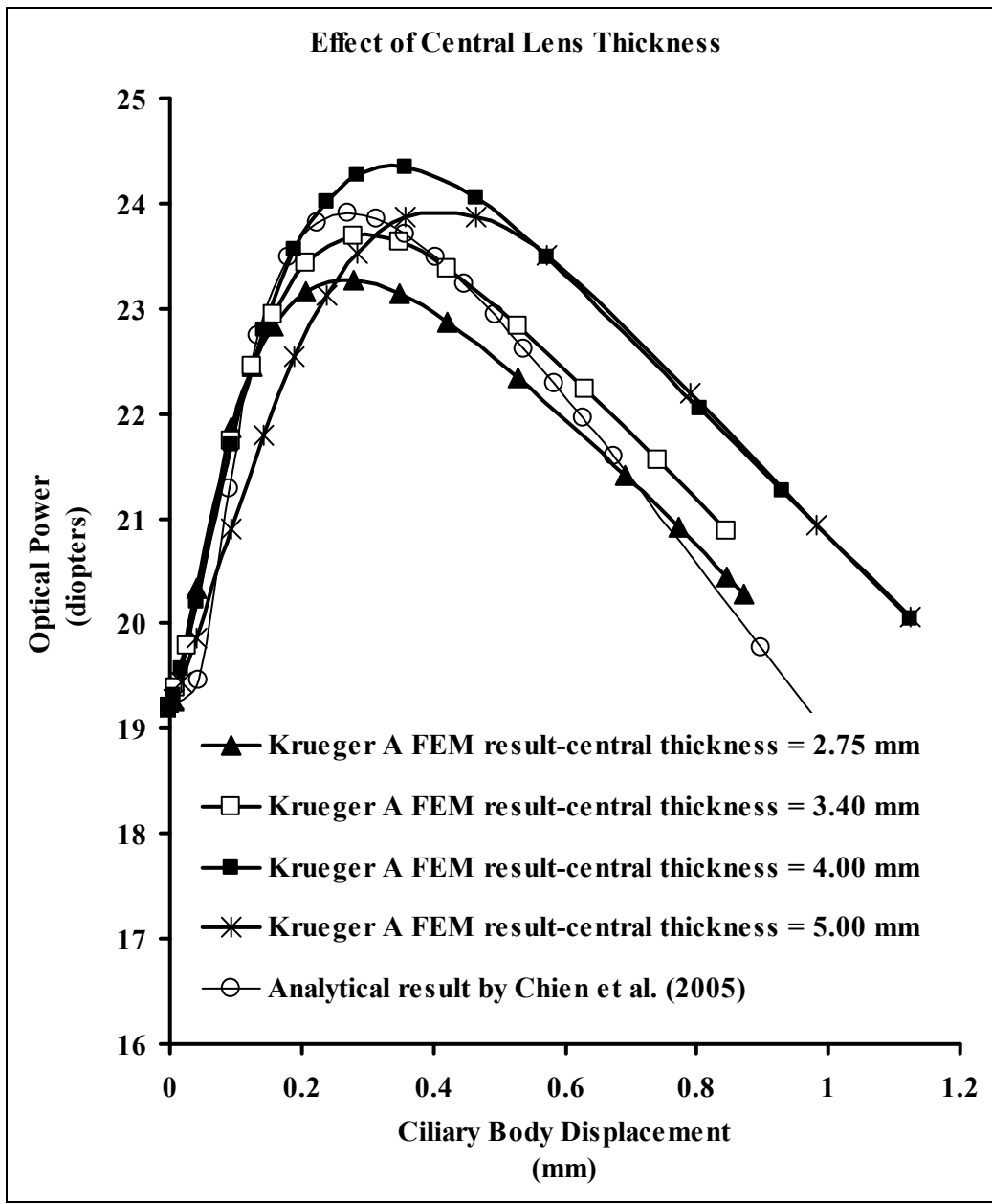
Figure A.7 Change in central thickness of lens
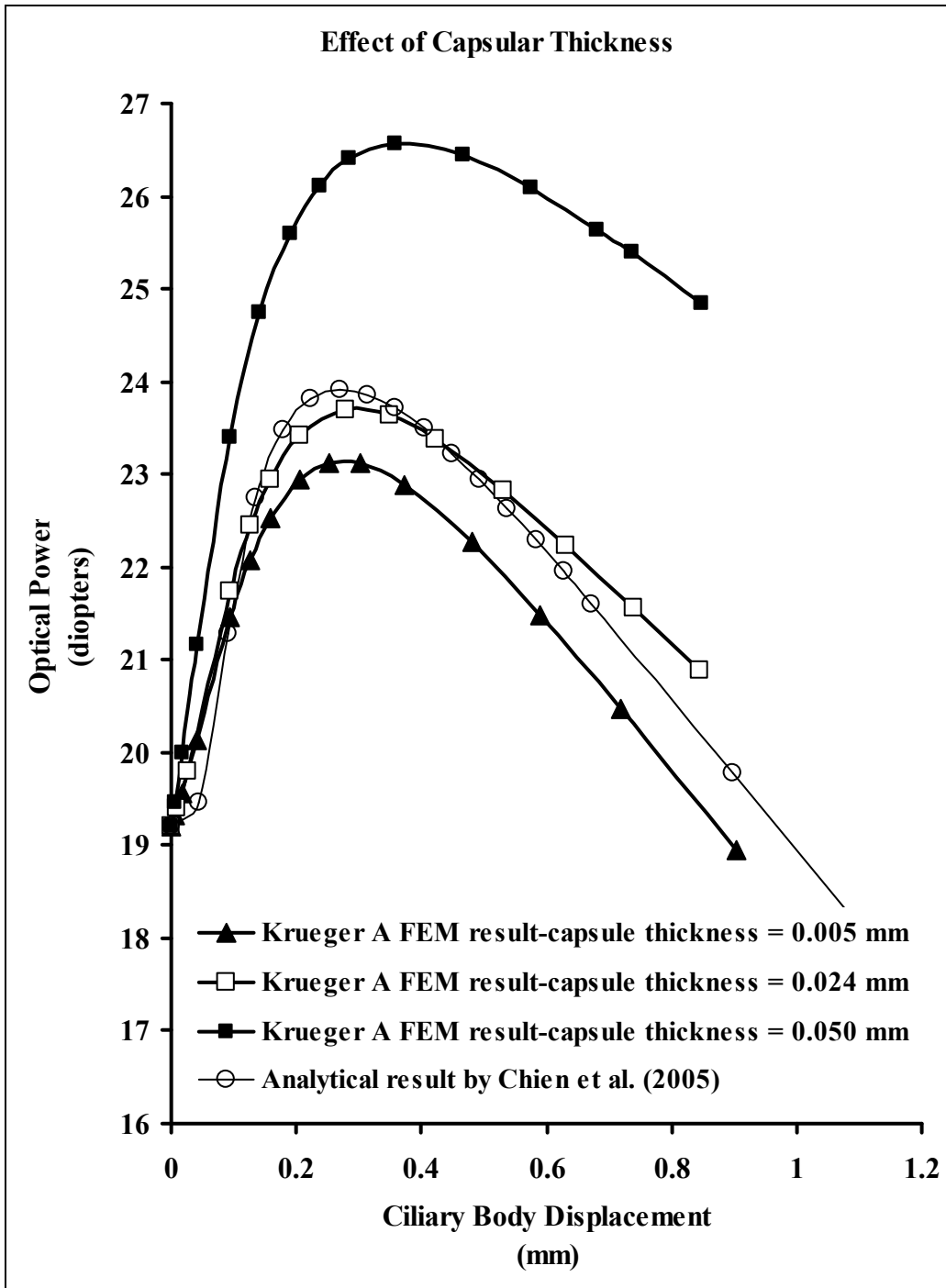
Figure A.8 Change in capsule thickness
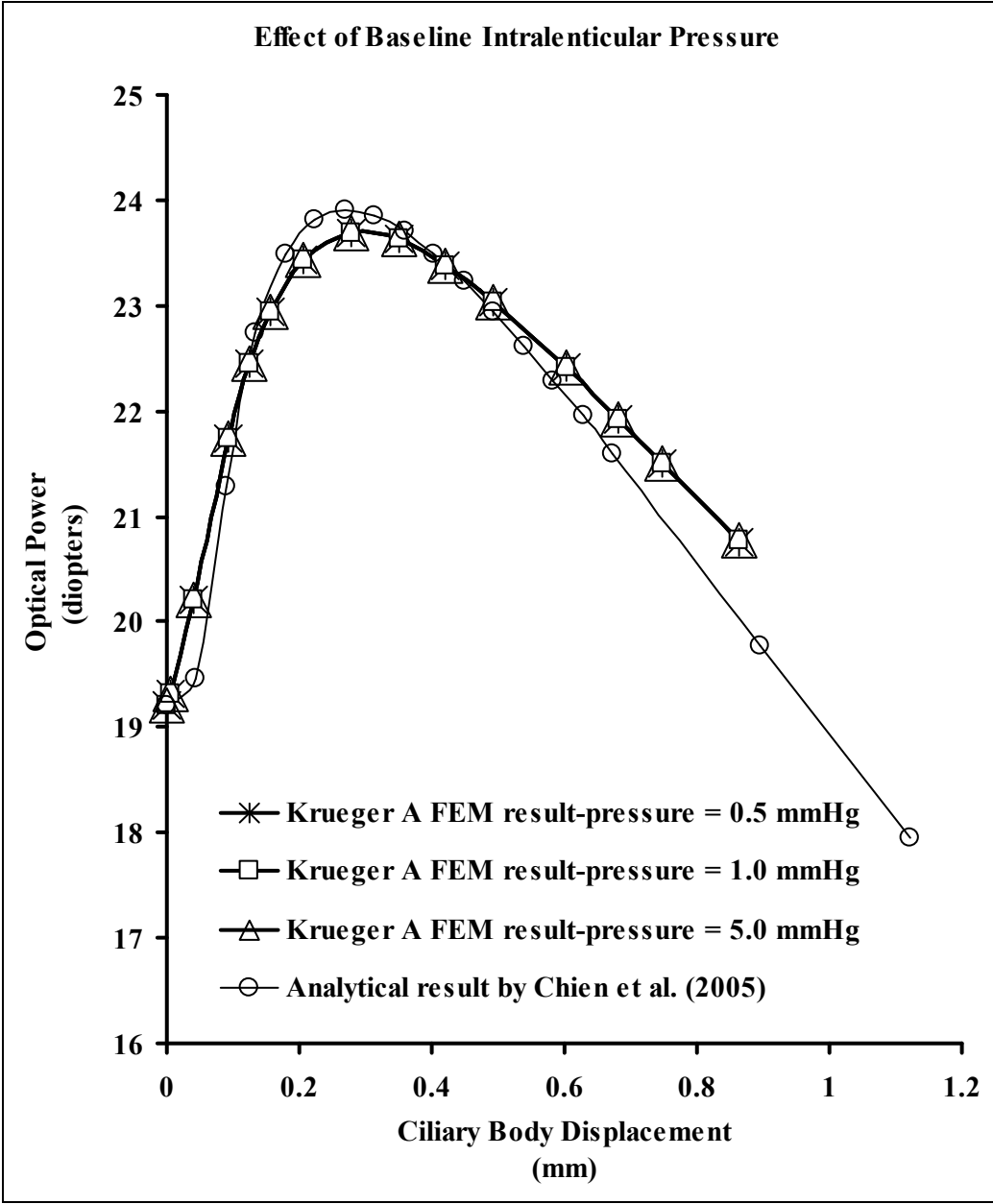
Figure A.9 Pressure was applied to the lens

Effect of Contact Elements Between Cortex and Nucleus

Contact Element : Normal Stiffness / Friction

- Krueger A FEM result with contact = 10/2.0
- Krueger A FEM result with contact = 8.0/2.0
- Krueger A FEM result with contact = 1.0/2.0
- Krueger A FEM result with contact = 0.5/2.0
- Krueger A FEM result with contact = 0.5/1.0
- Krueger A FEM result with contact = 0.1/0.2
- Krueger A FEM result no contact
- Analytical result by Chien et al. (2005)

Y-axis: **Optical Power (diopters)**

X-axis: **Ciliary Body Displacement (mm)**

Figure A.10 Contact elements are applied to lens between cortex and nucleus
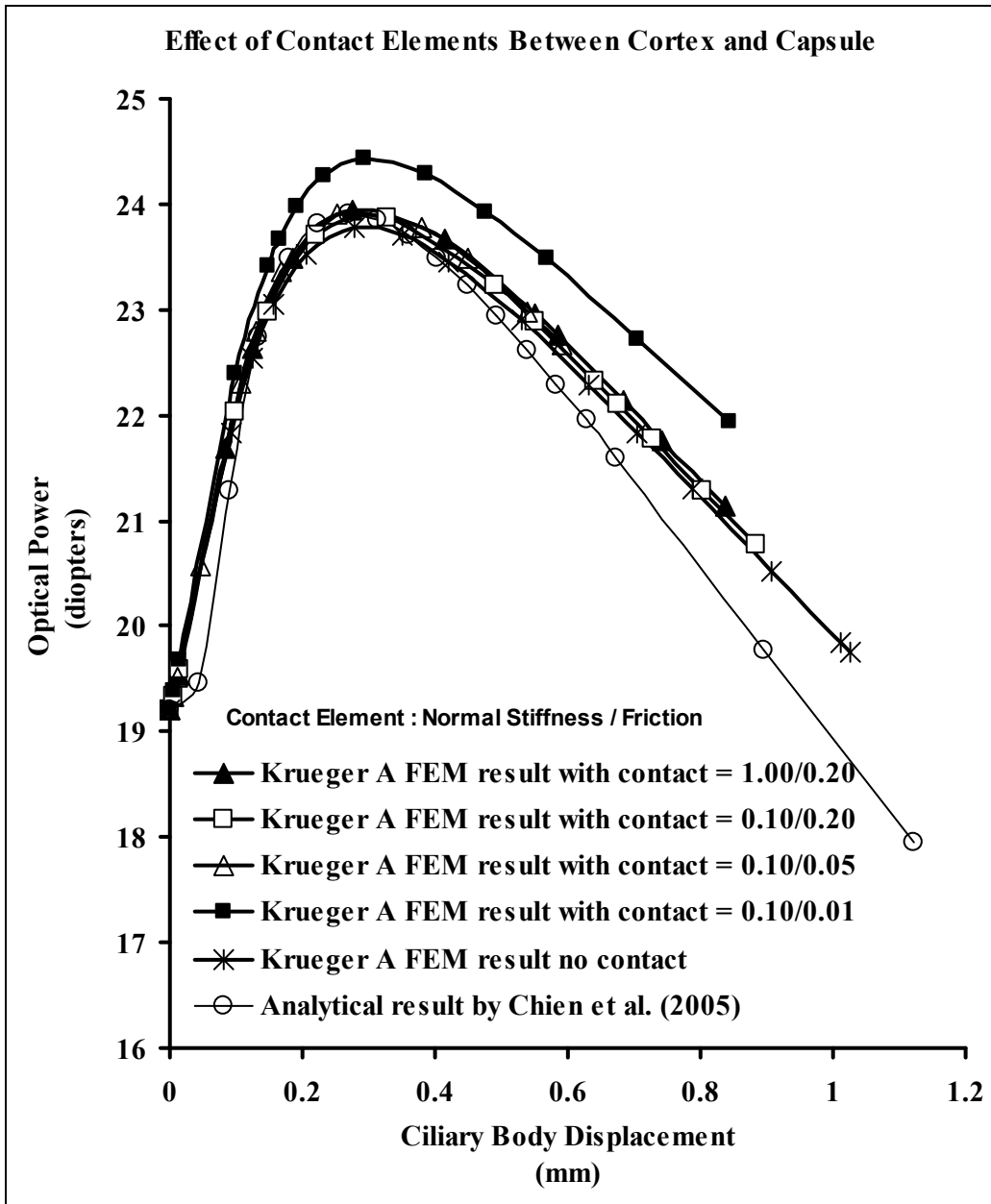
Figure A.11 Contact elements are applied to lens between cortex and capsule
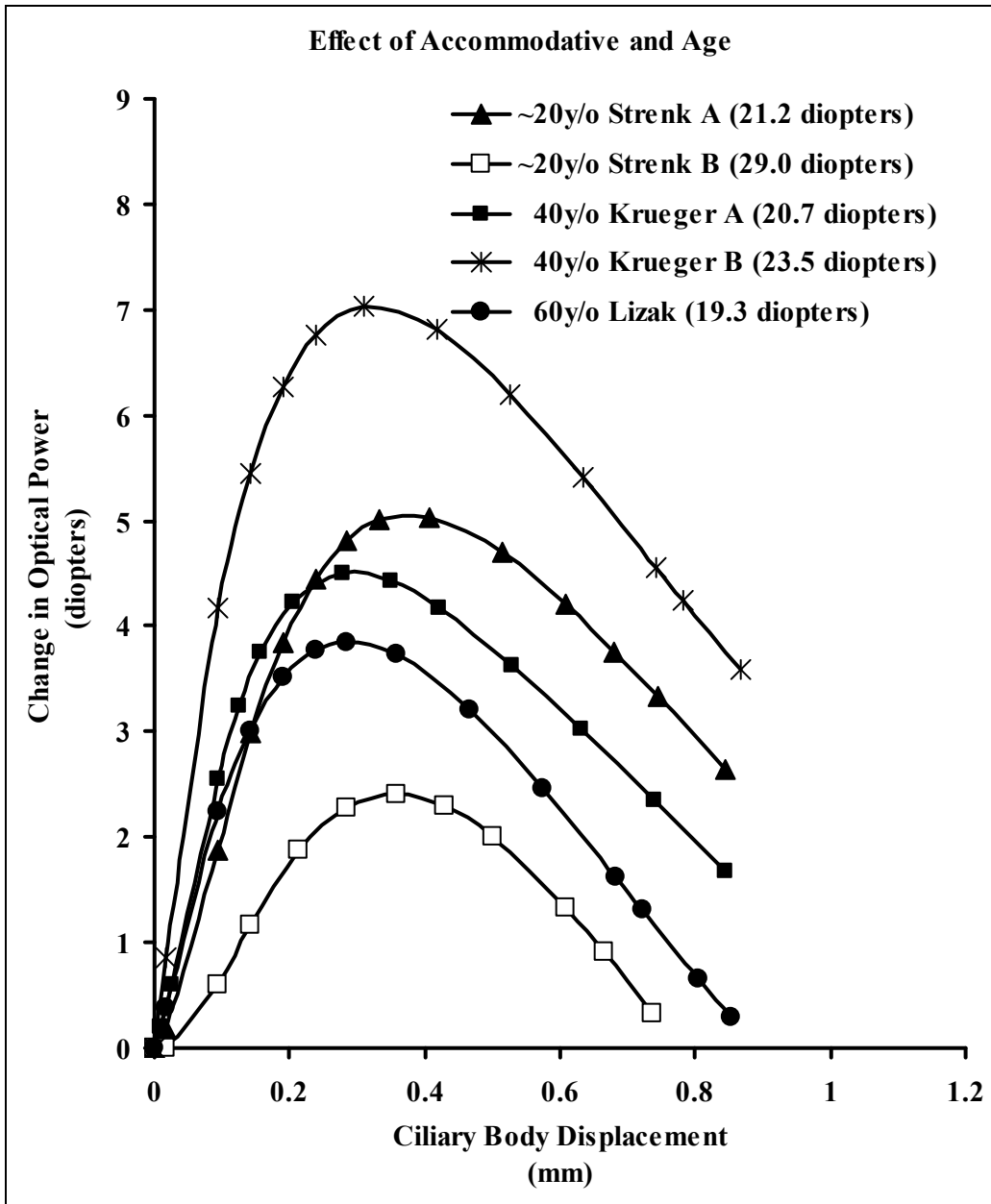
Figure A.12 Optical power due to accommodative stages and age
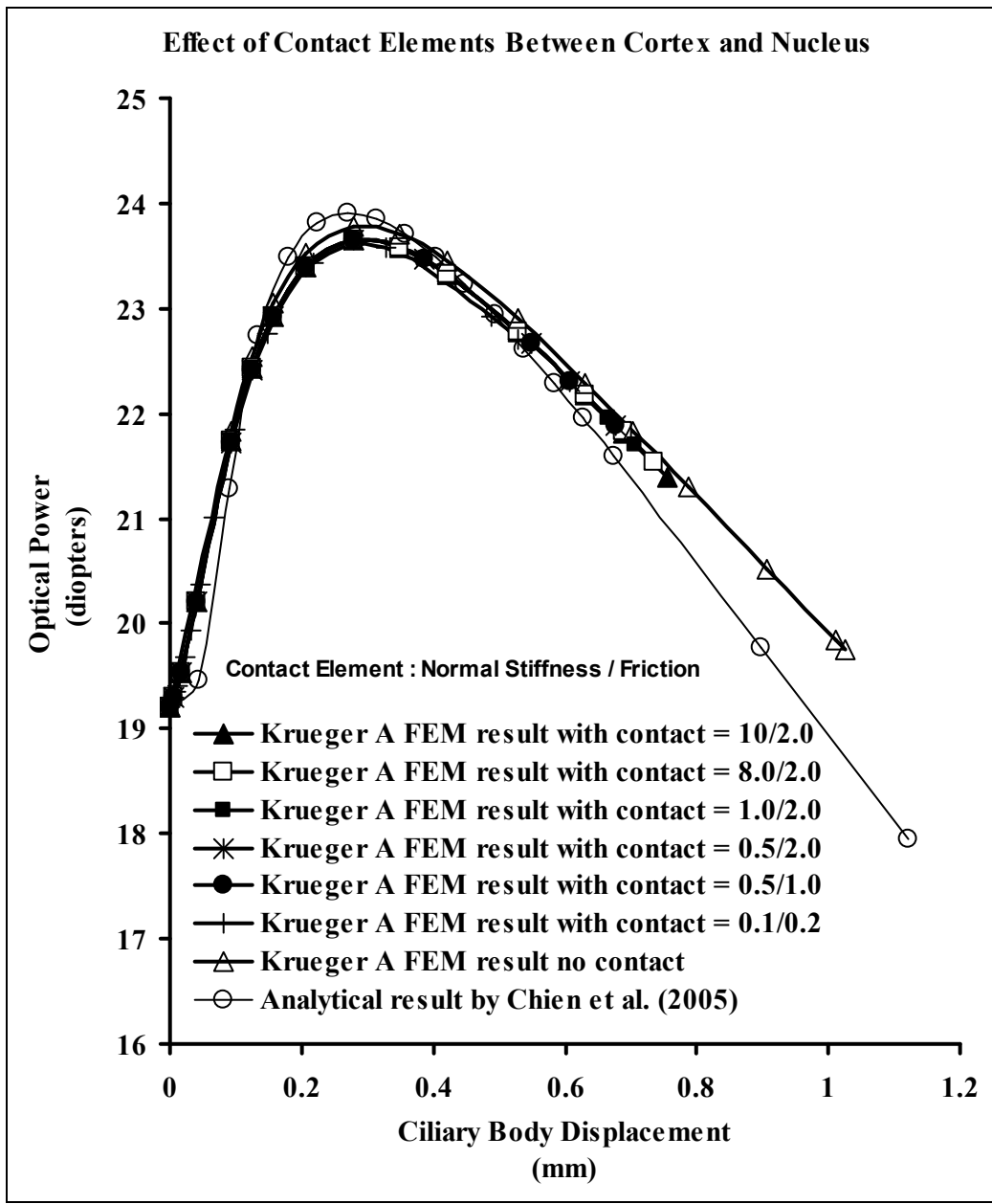
Effect of Location of Zonule Attachment

Position of zonules attachment from equator to : anterior/posterior (mm)

- Krueger A FEM result with 3 zonules at 1.00/0.75
- Krueger A FEM result with 3 zonules at 0.75/0.50
- Krueger A FEM result with 3 zonules at 0.50/0.25
- Krueger A FEM result with 2 zonules at 1.50/1.00
- Krueger A FEM result with 2 zonules at 1.00/0.50
- Krueger A FEM result with 2 zonules at 0.50/0.25
- Krueger A FEM result with 1 equatorial zonule
- Analytical result by Chien et al. (2005)

Optical Power (diopters)

Ciliary Body Displacement (mm)

Figure A.13 Effect of zonules attachment

Figure A.14 Effect of zonular traction on central thickness

Figure A.15 Effect of zonular traction on force and optical power

Figure A.16 Optical power with triangular element in capsule

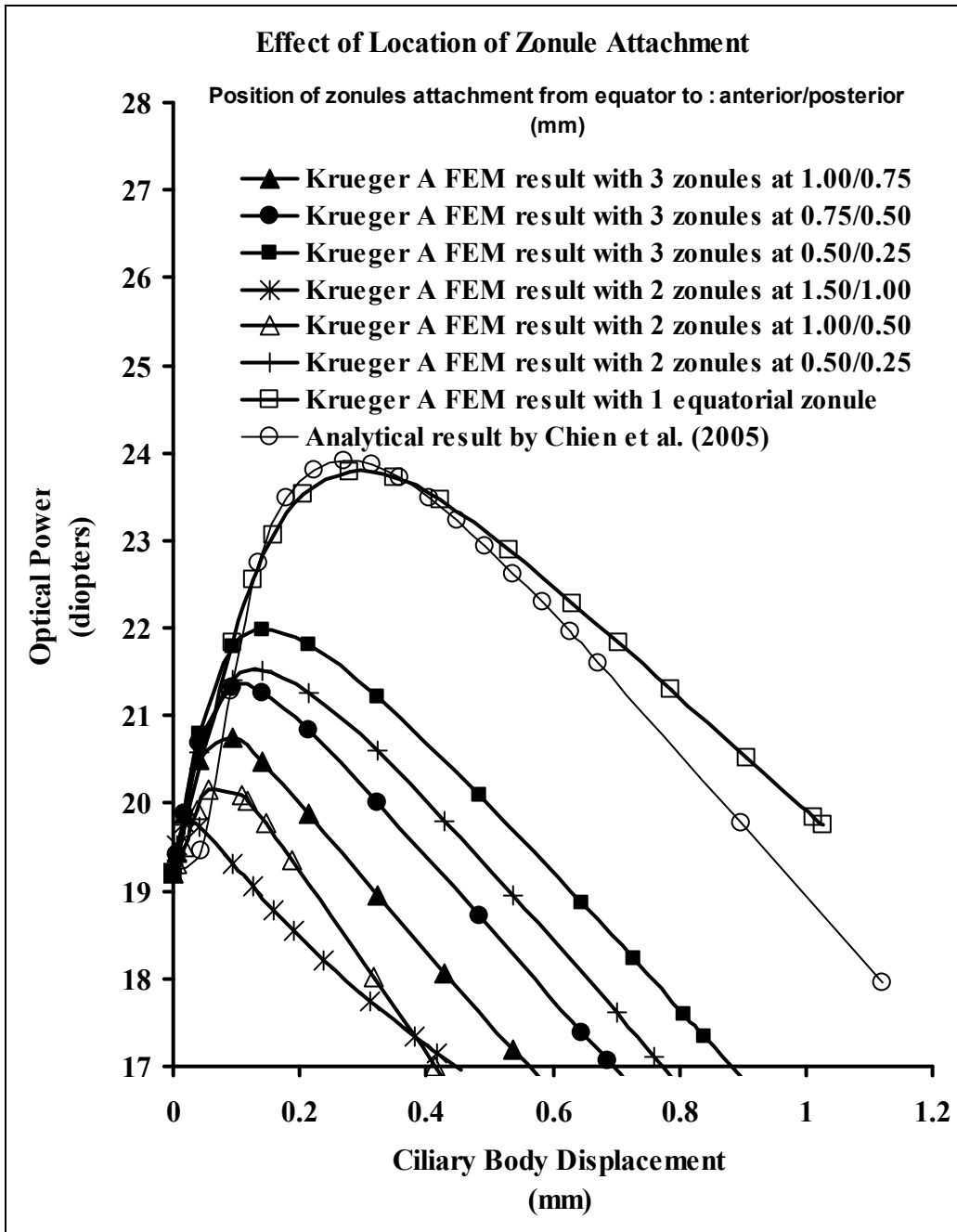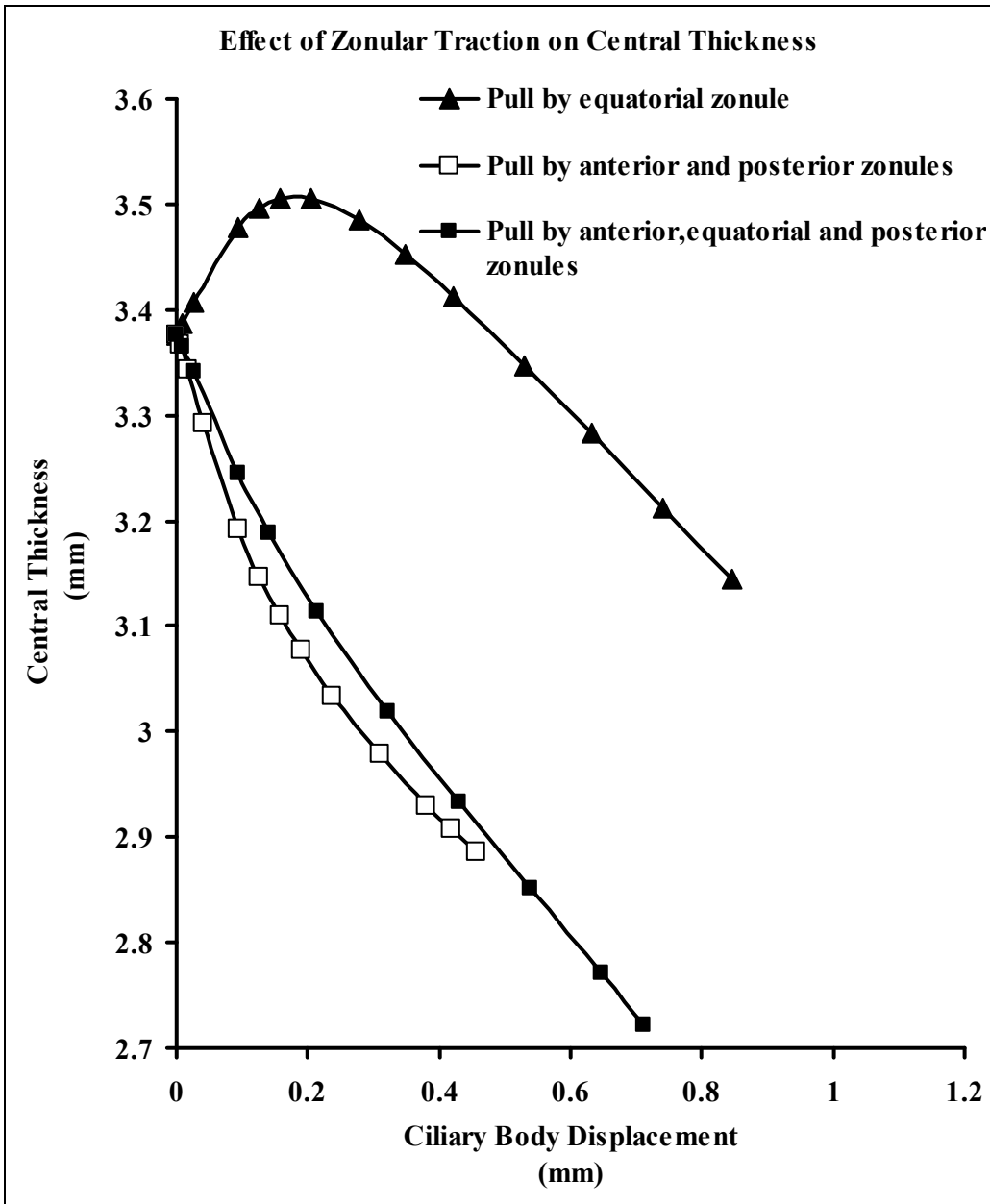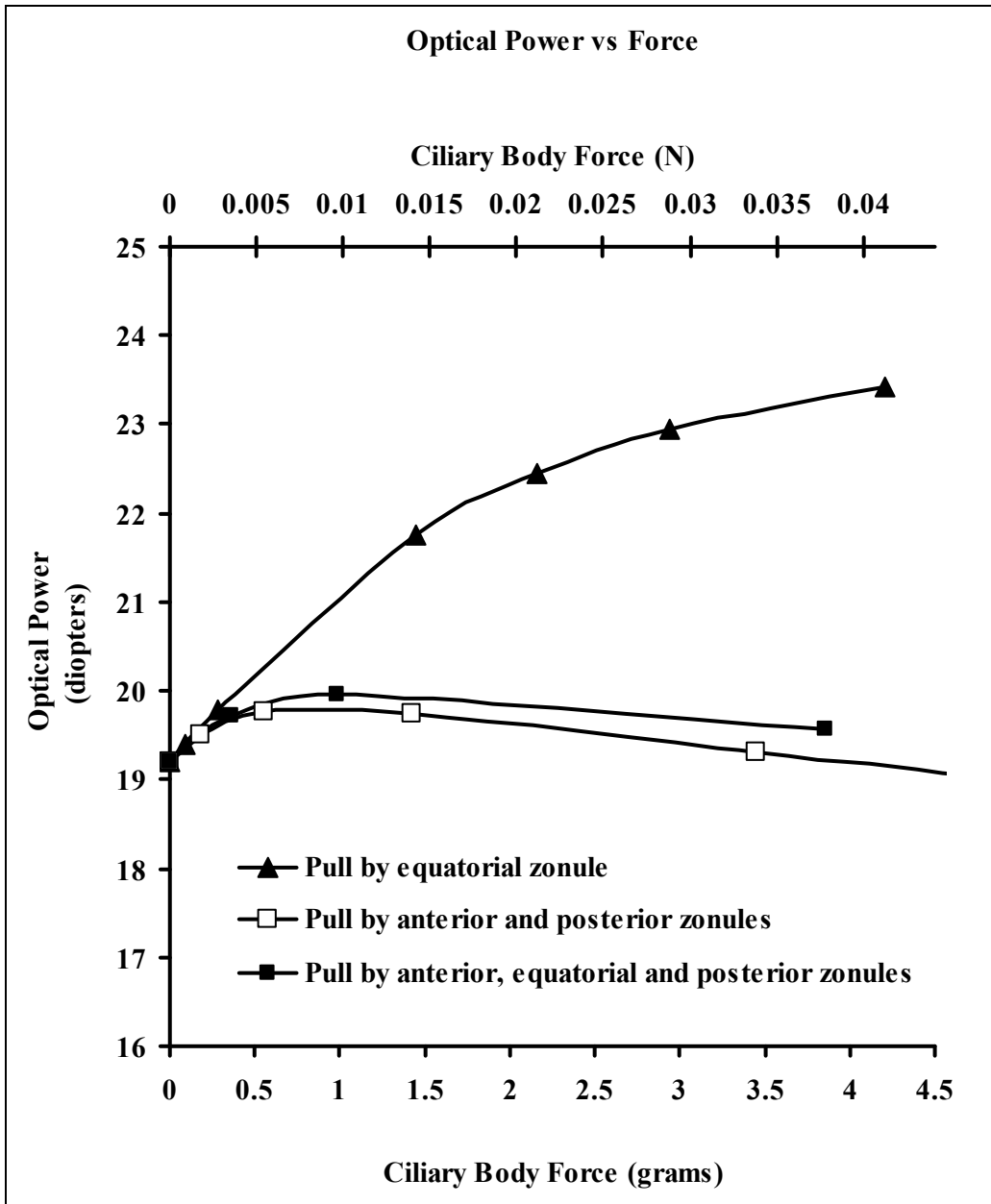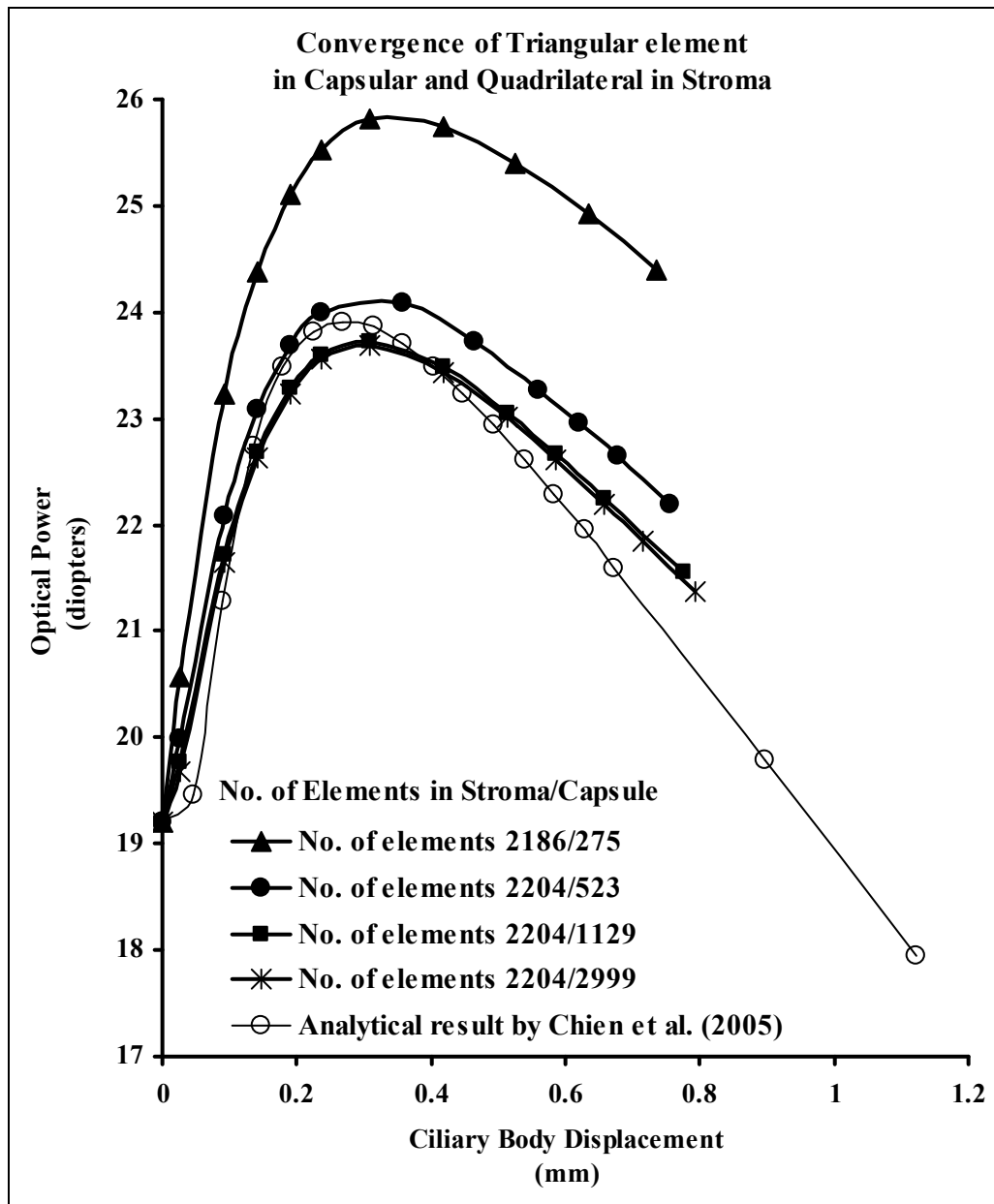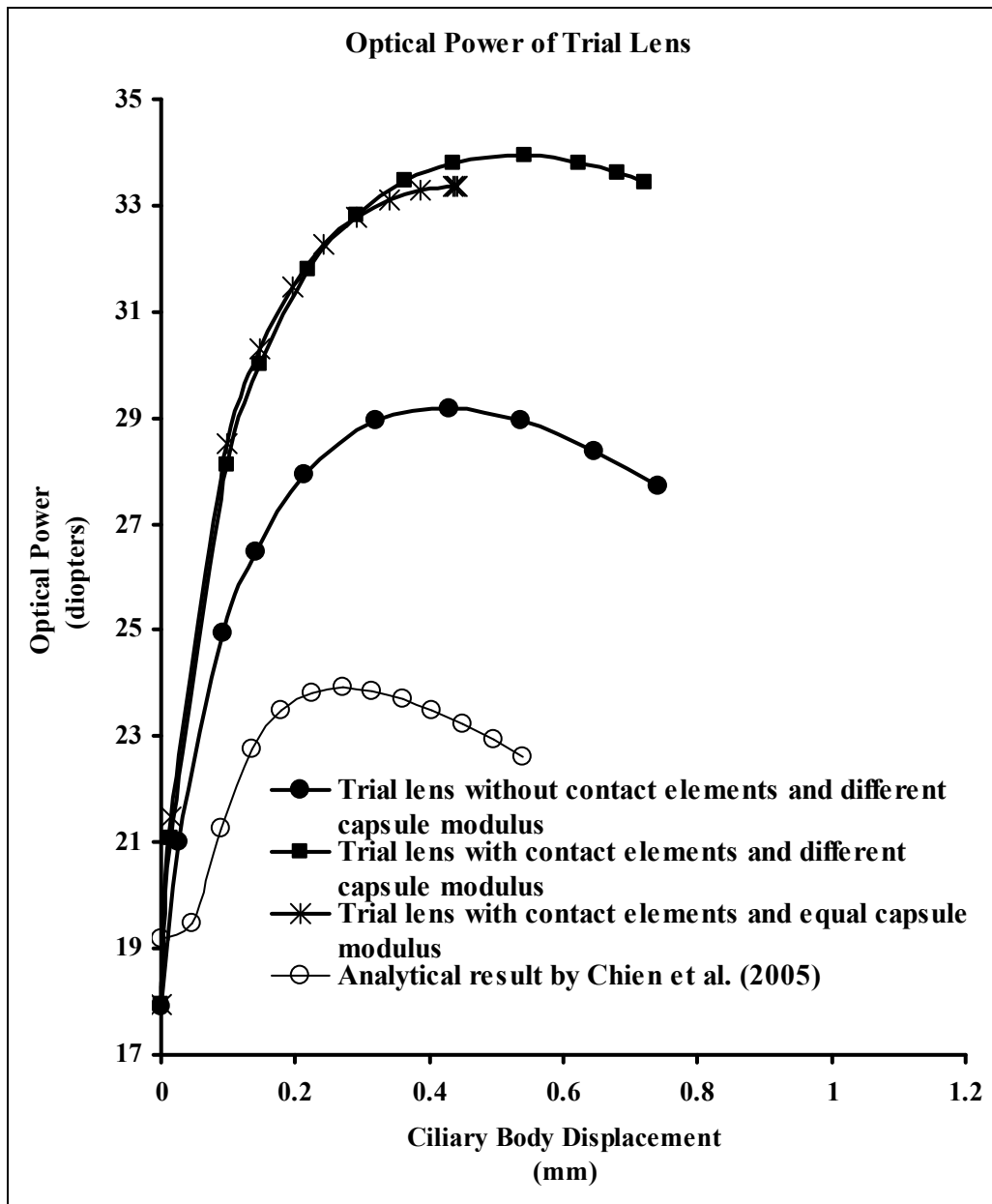Figure A.17 Optical power of the Trial lens with contact and without contact
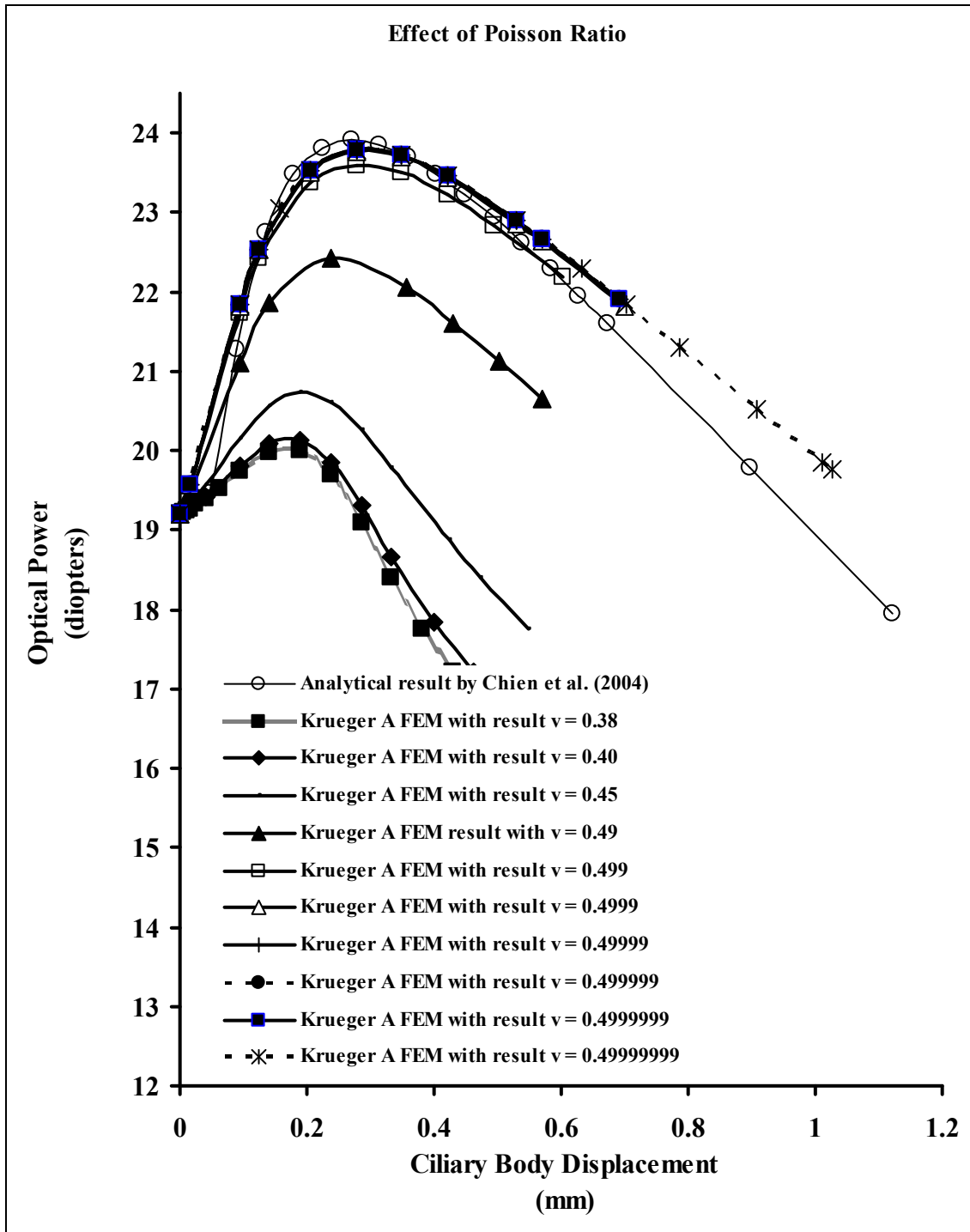
Figure A.18 Effect of compressibility on Optical power

REFERENCES

ABAQUS, 2005. ABAQUS version 6.5, ABAQUS, Inc., Pawtucket, RI.

Adler, F. H. 1950. Physiology of the Eye: Clinical Application. St. Louis Missouri: C.V. Mosby Company.

Alpern, M. 1969.Accommodation. in: Davson H. (Ed). The Eye; Muscular Mechanisms. New York: Academic Press. Vol. 3.

Blacker, T. D., and Stephenson M. B. Paving: a new approach to automated quadrilateral mesh generation. International Journal for Numerical Methods in Engineering 1991; 32:811–847.

Bowman, W. 1849. Lectures on the Parts concerned in the Operations of the Eye. London.pp.62.

Brown, N. 1974. The shape of the lens equator. Exp Eye Res 19(6): 571-6. Medline

Brucke, E. 1846 Arch. Anat. Physiol. wiss. Med.pp.370.

Burd, H. J., Judge, S. J., and Cross, J. A. 2002. Numerical modelling of the accommodating lens. Vis Res 42(18): 2235-51. Medline

Cass, R. J., Benzley, S.E., Mayers R. J., and Blacker, T. D. Generalized 3-D paving: an automated quadrilateral surface mesh generation algorithm. International Journal for Numerical Methods in Engineering 1996; 39:1475–1489.

Chien, C. H., Huang, T., and Schachar, R. A. 2005. Analysis of human crystalline lens accommodation. J Biomech In press.

Clough, R. W. 1960. The finite element method in plane stree analysis. Proceedings of the American Society of Engineers, 2nd Conference on Electronic Computations. Pittsburgh, Pennsylvania. Vol. 23: 345-378.

Clough, R. W. 1963. Stress analysis of a granity dam by finite element method. Proceedings of the Symposium on the Use of Computers in Civil Engineering. Laboratorio Nacional de Engenharia Civil, Lisbon, Portugal.

Clough, R. W. 1965. The finite element method in structural mechanics. In: Stress Analysis. New York: Wiley

Clough, R. W. 2004. Early history of the finite element method from the view point of a pioneer. International J Numerical Methods in Engineering60:283-287.

Coleman, D. J., and Fish, S. K. 2001. Presbyopia, accommodation, and the mature catenary. Ophthalmology 108(9): 1544-51 Medline

Courant, R. 1943. Variational methods for the solution of problems of equilibrium and vibrations. Bull Am Math Soc. 49: 1-23.

Cramer, A.1851. Ned. Lancet.;1:529.

Cramer, A. 1853 Het Accommodatievermogen der Oogen Physiologisch Tægelicht. Haarlem: de Erven Loosjes. 1853.

Descartes, R. 1677. Traité de l'homme. Paris

Donders, F.C. 1864. On the Anomalies of Accommodation and Refraction of the Eye. London, The Sydenham Society, 1864, pp 204-214

Donders, F. C. On the Anomalies of Accommodation and Refraction of the Eye. London, The New Sydenham Society. 1864;204-214.

Duane, A. 1917. Textbook of Ophthalmology. Philadelphia, Pennsylvania, J. B. Lippencott Company, ed 5, pp 859-863.

Dubbelman, M., Van der Heijde, G. L., and Weeber, H. A. 2005. Change in shape of the aging human crystalline lens with accommodation. <u>Vis Res 45(1)</u>: 117-32, 2005 Medline

Dugas, R. A History of Mathematics. <u>New York: Dover Publications, Inc</u>.

Duke, E. S., and Abrams. 1970. Ophthalmic Optics and Refracton. in: Duke Elder S (ed): System of Ophthalmology. <u>London, Henry Kimpton</u>. Vol. V.

Duke, E. S.,Gloster, J., and Weale, R. 1961.The physiology of the Eye and of Vision. in: Duke Elder S (ed): System of Ophthalmology, <u>London, Henry Kimpton</u>. Vol. IV.

Duke, E. S., and Waybar, K.C. 1961. The anatomy of the visual system, in: Duke Elder S (ed): System of Ophthalmology, <u>London, Henry Kimpton</u>. Vol. II.

Farnsworth, P. N., and Burke, P. 1977. Three-dimensional architecture of the suspensory apparatus of the lens of the Rhesus monkey. <u>Exp Eye Res 25(6)</u>: 563-76. Medline

Farnsworth, P. N., and Shyne, S. E. 1979. Anterior zonular shifts with age. <u>Exp Eye Res 28(3)</u>: 291-7 Medline

Fincham, E. F. 1937. The mechanism of accommodation. <u>Brit J Ophthalmol. suppl</u>. 8:1-80.

Gullstrand, A. 1911. Einfuhrung in d. Methoden d. <u>Dioptrik d. Auges d. Menschen. Leipzig</u>.

Hazel, C. A, Cox, M. J., and Strang, N. C. 2003 Wavefront aberration and its relationship to the accommodative stimulus-response function in myopic subjects. <u>Optom Vis Sci 200380(2)</u>: 151-8. Medline

Heys, K. R., Cram, S. L., and Truscott, R. J. 2004. Massive increase in the stiffness of the human lens nucleus with age: the basis for presbyopia? Mol Vis 10: 956-63. Medline

Hjort. 1876. Klin Monatsbl.f.Augenheilk p.205.

Hogan, M. J., Alvarado, J. A., and Weddell, J. E. 1971. Histology of the Human Eye. Philadelphia, Pennsylvania, WB. Saunders Company, pp 638-677

Hrennikoff, A. 1941. Solution of problems in elasticity by the framework method. J Appl Mech. 8: A169-A175.

Jaffe, N. S. 1976. Cataract Surgery and its Complications. St. Louis, Missouri, The C. V. Mosby Company, ed 2. pp 83-98

Johnston, B. P., Sullivan, J. M. Jr., and Kwasnik, A. Automatic conversion of triangular _nite element meshes to quadrilateral elements. International Journal for Numerical Methods in Engineering 1991; 31:67–84.

Kaufman, P. L., Rohen, J. W., and Barany E. H.. 1979. Hyperopia and loss of accommodation following ciliary muscle disinsertion in the cynomolgus monkey: physiologic and scanning electron microscopic studies. Invest Ophthalmol Vis Sci 18(7): 665-73, Medline

Kepler, J. 1611. Dioptrice. Augsburg

Koeppl, C., Findl, O., and Kriechbaum, K., et al. 2005. Comparison of pilocarpine-induced and stimulus-driven accommodation in phakic eyes. Exp Eye Res 80(6): 795-800. Medline

Kolker, A. E., and Hetherington, Jr. J. 1970. Becker-Shaffer's Diagnosis and Therapy of the Glaucomas. 3rd Edition. St. Louis:C.V. Mosby Company.

Krag, S., and Andreassen, T. T. 2003. Mechanical properties of the human posterior lens capsule. Invest Ophthalmol Vis Sci 44(2): 691-96 Medline

Krag, S., and Andreassen, T. T. 2003. Mechanical properties of the human lens capsule. Prog Retin Eye Res 22(6) 749-67. Medline

Kriechbaum, K., Findl, O., and Koeppl C. et al. 2005. Stimulus-driven versus pilocarpine-induced biometric changes in pseudophakic eyes. Ophthalmology. 112(3):453-9. Medline

Kuszak, J. R., Zoltoski, R. K., and Sivertson, C. 2004. Fibre cell organization in crystalline lenses. Exp Eye Res 78: 673-87. Medline

Langenbeck, M. 1849. Klin. Beitr. A. d. Gebiete d. Chirurgie u. Ophthal. Göttingen.

Landolt, E. 1886. The Refraction and Accommodation of the Eye. Translator: Culver CM. Edinburgh: Young J Pentland.

Levy, S. 1953. Structural analysis and influence coefficients for Delta wings. J Aeronaut Sci 20: 449-454

Li, Y., and Chalta, M. R., 2005. Huang D: Measurement of lens curvature change during accommodation with high-speed optical coherence tomography. Association for Research in Vision and Ophthalmology Meeting, Abstract # 2554. http://www.abstractsonline.com/viewer/SearchResults.asp

Lo, S. H. A new mesh generation scheme for arbitrary planar domain. International Journal for Numerical Methods in Engineering 1985; 21:1403–1426.

Lograno, M. D., and Reibaldi, A. 1986. Receptor-responses in fresh human ciliary muscle. : Br J Pharmacol 87(2): 379-85. Medline.

Mann, I. 1969. The Development of the Human Eye. New York, Grune & Stratton, Inc., pp 46-67

Ninomiya, S., Fujikado, T., and Kuroda, T., 2002. Changes of ocular aberration with accommodation. Am J Ophthalmol 134(6): 924-6. Medline

Ophthalmol. 28:70-79.

Ogle, K. N. 1968. Optics. 2nd Edition. Sprinfield, Illinois: Charles C. Thomas, Publisher.

Patankar, S. V. 1991. Numerical heat transfer and fluid flow. New York: McGraw-Hill,.

Pierscionek, B. 1993. In vitro alteration of human lens curvature by radial stretching. Exp Eye Res 57(5): 629-635. [Central steepening secondary to zonular traction is determined by calculating the radius of curvature at x = 0 from the quadratic formulas given for the 27-year-old lens in Table 1]. Medline

Purkinge, J. E.1823. Beobachtungen u. Versuche z. Physiologie d. Sinne. Prague.2:128.

Rohen, J. W. 1979. Scanning electron microscopic studies of the zonular apparatus in human and monkey eyes. Invest Ophthalmol Vis Sci 18(2):133-44 Medline

Sarfarazi, M. F. 2005. New look at the mechanism of accommodation. American Society of Cataract and Refractive Surgery Meeting, Session 1-E, April 16, 2005. Abstract

Schachar, R. A. 1992. Cause and treatment of presbyopia with a method for increasing the amplitude of accommodation. Ann Ophthalmol 24(12): 445-7, 452, 1992 Medline

Schachar, R. A. 1994a. Pathophysiology of Accommodation and Presbyopia: Understanding the Clinical Implications. J Florida M.A. 81:268-271.

Schachar, R. A. 1994. Zonular function: a new hypothesis with clinical implications. Ann Ophthalmol 26(2): 36-8, 1994 Medline

Schachar, R. A. 1996. Histology of the ciliary muscle-zonular connections. <u>Ann Ophthalmol 28</u>: 70-9, 1996 http://www.2ras.com/12.pdf

Schachar, R. A. 1999. Is Helmholtz's Theory of Accommodation Correct? <u>Ann Ophthalmol 31</u>: 10-7. http://www.2ras.com/15.pdf

Schachar, R. A. 2001. The correction of presbyopia. <u>Int Clin Ophthalmol. 41(2)</u>: 53-70.

Schachar, R. A. 2002a. Presbyopic surgery. <u>Int Ophthalmol Clin 42(4)</u>: 107-18, 2002. Medline

Schachar, R. A. 2002b. The mechanism of accommodation and presbyopia, in Agarwal A. (ed): Presbyopia: A Surgical Textbook, Thorofare, <u>New Jersey, Slack Inc</u>. pp 37-49.

Schachar, R. A. 2004. Central surface curvatures of postmortem-extracted intact human crystalline lenses: implications for understanding the mechanism of accommodation. <u>Ophthalmology 111(9)</u>: 1699-1704. <u>Medline</u>

Schachar, R. A. 2004. Qualitative effect of zonular tension on freshly extracted intact human crystalline lenses: implications for the mechanism of accommodation. <u>Invest Ophthalmol Vis Sci 45(8)</u>: 2691-5. <u>Medline</u>

Schachar, R. A. 2005a. Growth patterns of fresh human crystalline lenses measured by in vitro photographic biometry. <u>J Anat 206</u>: 575-580.

Schachar, R. A. 2005b. The mechanism of accommodation and presbyopia. Submitted.

Schachar, R. A., and Anderson, D. A. 1995. The mechanism of ciliary muscle function. <u>Ann Ophthalmol 27: 126-32</u>. http://www.2ras.com/9.pdf

Schachar, R. A., and Bax, A. J. 2001. Mechanism of human accommodation as analyzed by nonlinear finite element analysis. <u>Compr Ther 27(2)</u>: 122-32. Medline

Schachar, R. A., Black, T. D., and Kash, R. L., et al. 1995. The mechanism of accommodation and presbyopia in the primate. Ann Ophthalmol 27: 58-67. http://www.2ras.com/8.pdf.

Schachar, R. A., Cudmore, D. P., and Black T. D. et al.1998. Paradoxical optical power increase of a deformable lens by equatorial stretching. Ann Ophthalmol 30: 10-8, 1998 http://www.2ras.com/14.pdf

Schachar, R. A., Cudmore, D. P., and Torti, R., et al. 1994. A physical model demonstrating Schachar's hypothesis of accommodation. Ann Ophthalmol 26: 4-9, 1994 Medline

Schachar, R. A., Huang T., and Huang, X. 1993. Mathematic proof of Schachar's hypothesis of accommodation. Ann Ophthalmol 25(1): 5-9. Medline

Schachar, R. A., and Kamangar, F. 2005. Computer image analysis of ultrasound biomicroscopy of primate accommodation. Eye Apr 8 [Epub ahead of print]. Medline

Schachar, R. A., and Solin, S. A. 1975. The microscopic protein structure of the lens with a theory for cataract formation as determined by Raman spectroscopy of intact bovine lenses. Invest Ophthalmol 14(5): 380-96, 1975 Medline

Schachar, R. A., Tello C., and Cudmore, D. P., et al. 1996. In vivo increase of the human lens equatorial diameter during accommodation. Am J Physiol 271(3 Pt 2) R670-6. Medline

Scheiner, C. 1619 Oculus. Innsbruck

Shung, W. V. 2002. An analysis of a crystalline lens subjected to equatorial periodic pulls. PhD. Thesis, University of Texas at Arlington, Texas.

Stadfeldt, A. E. 1896. Di veränderung der lines bei traction der zonula. Klin Monatsbl Augenheilkd 34: 429-31.

Streeten, B. W. 1982a. The nature of the ocular zonule. <u>Trans Am Ophthalmol Soc 80: 823-54</u>. <u>Medline</u>

Streeten, B. W. 1982b. Zonular apparatus, in: Jakobiec FA (ed): Ocular Anatomy Embryology and Teratolog,. <u>Philadelphia, Pennsylvania, Harper and Row, 1982</u>, pp 331-353

Strenk, S. A., Semmlow, J. L., and Strenk, L. M., et al. 1999. Age-related changes in human ciliary muscle and lens: a magnetic resonance imaging study. <u>Invest Ophthalmol Vis Sci 40(6)</u>: 1162-9. Medline

Strenk, S. A., Strenk, L. M., and Koretz, J. F., et al. 2005. Change in Intralenticular Pressure during Accommodation, eLetter. <u>Invest Ophthalmol Vis Sci March 30, 2005</u>. http://www.iovs.org/cgi/eletters/45/2/539

Strenk, S. A., Strenk, L. M., and Koretz, J. F. 2005. The mechanism of presbyopia. <u>Prog Retin Eye Res 24(3)</u>: 379-93. <u>Medline</u>

Sturm, J. C. 1697. Dissertatio de presbyopia et myopia Altdorfii

Talbert, J. A., and Parkinson, A. R. Development of an automatic two dimensional _nite element mesh generator using quadrilateral elements and Bezier curve boundary de_nition. <u>International Journal for Numerical Methods in Engineering 1991</u>; 29:1551–1567.

Tamm, E., Croft, M. A., and Jungkunz, W., et al. 1992. Age-related loss of ciliary muscle mobility in the rhesus monkey. Role of the choroid. <u>Arch Ophthalmol 110(6)</u>: 871-6, <u>Medline</u>

Thomas, C. L. Editor. 13th Edition. Taber's Cyclopedic Medical Dictionary

Tscherning, M. 1904. Physiological Optics. <u>Philadelphia, Pa. Keystone</u>.160-189.

van Alphen, G. W., Robinette, S. L., and Marci, F. J. 1962. Drug effects on ciliary muscle and choroid preparations in vitro. <u>Arch Ophthalmol 68: 81-93</u>. <u>Medline</u>

98

von Graefe, A. 1860. Fall von acquirirter Aniridie als Beitrag zur Accommodationslehre. <u>Archiv für Ophthalmologie, B. 7</u>:150-161.

von Helmholtz, H. 1855. Uber die akkommodation des auges. Albrecht von graefes <u>Arch Ophthalmol</u>.;1:1-89.

Weale, R. A. 1982. A Biography of the Eye: Development, Growth, Age. <u>London, H.K. Lewis</u>.

White, D. R., and Kinney, P. Redesign of the paving algorithm: robustness enhancements through element by element meshing. Proceedings of the 6th International Meshing Roundtable, <u>Park City, Utah, U.S.A. 1997</u>, 323–335.

Wilson, E. L. 1993. Automation of the finite element method, a personal historical view. <u>Finite Element in Analysis and Design. 13</u>: 91-104

Young, T. 1801. On the mechanism of the eye. <u>Phil Trans Roy Soc. 92</u>:23-88.

Zhu, J. Z., Zienkiewicz, O. C., Hinton, E., and Wu, J. A new approach to the development of automatic quadrilateral mesh generation. <u>International Journal for Numerical Methods in Engineering 1991</u>; 32:849–866.

Zienkiewicz, O. C. 1979. The Finite Element Method. <u>London: McGraw-Hill</u>.

Zienkiewicz, O. C., and Cheung, Y. K. K. 1967. The Finite Element Method in Structural and Continuous Mechanics. <u>London: McGraw-Hill</u>.

BIOGRAPHICAL INFORMATION

Tri Dai Le was born October 20, 1980 in Tien Giang province, Vietnam to Thanh Nguyen and Liet Le. He spent his childhood in a peaceful countryside in Mekong delta where he finished high school in 1997. Then he moved to Hochiminh, the largest and most crowded city in Vietnam, for his bachelor degree in Civil Engineering at the University of Technology, one of the famous universities in Vietnam. He graduated in 2002. Right after graduation, he worked for a state owned company for six months as a technician staff member who estimated building cost and prepared documents for tender. After that he worked for a British company, Atlas Co.Ltd., where he worked for 18 months as an AutoCAD detailer. Tri is became an expert in detailing reinforced slab and retaining wall drawings.

Afterward, he entered the graduate program in Structural and Applied Mechanics at the University of Texas at Arlington (UTA) where he did research under Dr. Ali Abolmaali instruction as a Master of Science in Civil Engineering in finite element method. Tri Le has been accepted to the Ph.D. program in structural mechanics at UTA and is awarded the Hermon Scholarship.